The Broad-lined Type Ic SN 2003jd[*]

S. Valenti[1,2]†, S. Benetti[3], E. Cappellaro[3], F. Patat[2], P. Mazzali [4,5], M. Turatto [3],
K. Hurley [6], K. Maeda [4,7], A. Gal-Yam[8], R. J. Foley[9], A. V. Filippenko[9],
A. Pastorello[10], P. Challis[11], F. Frontera [1,12], A. Harutyunyan [3], M. Iye[13],
K. Kawabata [14], R. P. Kirshner[11], W. Li [9], Y. M. Lipkin [15], T. Matheson[16],
K. Nomoto[17,18], E. O. Ofek[8], Y. Ohyama[19], E. Pian[5], M. Salvo[20], D. N. Sauer[4],
B. P. Schmidt[20], A. Soderberg [8], and L. Zampieri [3]

[1] *Physics Department, University of Ferrara, I-44100 Ferrara, Italy.*
[2] *European Organisation for Astronomical Research in the Southern Hemisphere, Karl-Schwarzschild Strasse 2,*
Garching bei München, D-85748, Germany.
[3] *INAF - Astronomical Observatory of Padova, I-Padova, Italy.*
[4] *Max-Planck Institut für Astrophysik, Karl-Schwarzschild Strasse 1, Garching bei München, D-85748, Germany.*
[5] *INAF - Osservatorio Astronomico, Via Tiepolo 11, 34143 Trieste, Italy.*
[6] *University of California, Space Sciences Laboratory, Berkeley, CA 94720-7450, USA.*
[7] *Department of Earth Science and Astronomy, College of Arts and Science, University of Tokyo, Meguro-ku, Tokyo 153-8902, Japan.*
[8] *Division of Physics, Mathematics and Astronomy, California Institute of Technology, Pasadena, CA 91125, USA.*
[9] *Department of Astronomy, University of California, Berkeley, CA 94720-3411, USA.*
[10] *Astrophysics Research Centre, School of Mathematics and Physics, Queen's University Belfast, Belfast BT7 1NN, United Kingdom.*
[11] *Harvard-Smithsonian Center for Astrophysics, 60 Garden Street, Cambridge, MA 02138, USA.*
[12] *INAF - Instituto di Astrofisica Spaziale e Fisica Cosmica Bologna, via P. Gobetti 101, 40129 Bologna, Italy.*
[13] *Division of Optical and Infrared Astronomy, NAOJ, Osawa 2-21-1, Mitaka, Tokyo 181-8588, Japan.*
[14] *Hiroshima Astrophysical Science Center, Hiroshima University, 1-3-1 Kagamiyama, Higashi-Hiroshima, Hiroshima 739-8526, Japan.*
[15] *School of Physics and Astronomy and Wise Observatory, Tel Aviv University, Tel Aviv 69978, Israel.*
[16] *National Optical Astronomy Observatory, 950 N. Cherry Ave., Tucson, AZ 85719-4933.*
[17] *Department of Astronomy, School of Science, University of Tokyo, Bunkyo-ku, Tokyo 113-0033, Japan.*
[18] *Research Center for the Early Universe, School of Science, University of Tokyo, Bunkyo-ku, Tokyo 113-0033, Japan.*
[19] *Department of Infrared Astrophysics, ISAS, Japan Aerospace Exploration Agency (JAXA), 3-1-1 Yoshinodai, Sagamihara,*
Kanagawa 229-8510, Japan.
[20] *Research School of Astronomy and Astrophysics, Australian National University, Mount Stromlo and Siding Spring Observatories,*
Cotter Road, Weston Creek, ACT 2611, Australia.

ABSTRACT

The results of a world-wide coordinated observational campaign on the broad-lined Type Ic SN 2003jd are presented. In total, 74 photometric data points and 26 spectra were collected using 11 different telescopes. SN 2003jd is one of the most luminous SN Ic ever observed. A comparison with other Type Ic supernovae (SNe Ic) confirms that SN 2003jd represents an intermediate case between broad-line events (2002ap, 2006aj), and highly energetic SNe (1997ef, 1998bw, 2003dh, 2003lw), with an ejected mass of $M_{ej} = 3.0 \pm 1$ M$_\odot$ and a kinetic energy of $E_k(\mathrm{tot}) = 7^{+3}_{-2} \times 10^{51}$ erg. SN 2003jd is similar to SN 1998bw in terms of overall luminosity, but it is closer to SNe 2006aj and 2002ap in terms of light-curve shape and spectral evolution. The comparison with other SNe Ic, suggests that the V-band light curves of SNe Ic can be partially homogenized by introducing a time stretch factor. Finally, due to the similarity of SN 2003jd to the SN 2006aj/XRF 060218 event, we discuss the possible connection of SN 2003jd with a GRB.

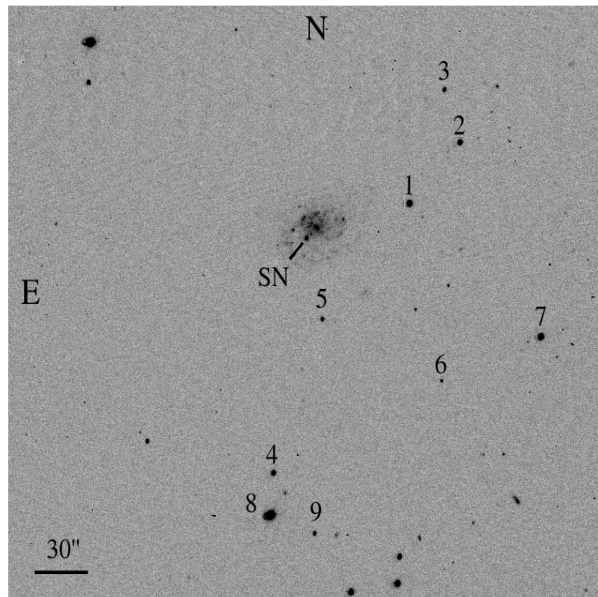**Key words:** Supernovae: general – individual SNe: 2003jd,1996aq – GRB connection

Figure 1. The field of SN 2003jd. *B*-band TNG image (14 Nov. 2003) 16.4 d after the *B* maximum.

1   INTRODUCTION

In the past decade, the discovery of the connection of some gamma-ray bursts (GRBs) with Type Ic supernovae (SNe Ic; see Filippenko 1997, for a review of supernova classification) boosted interest in the study of this type of SN (Galama et al. 1998; Stanek et al. 2003; Hjorth et al. 2003; Malesani et al. 2004; Pian et al. 2006; Soderberg et al. 2006; Campana et al. 2006).

In the current paradigm there is a distinction between *normal* SNe Ic of relatively low kinetic energy ($E_{51} = E_K/(10^{51}$ erg) ≈ 1; Nomoto et al. 2001), of which SN 1994I represents a prototype, and high-energy, broad-lined events like SN 1998bw ($E_{51} > 10$; Iwamoto et al. 1998; Maeda et al. 2002) which are associated with GRBs. To understand whether these are separate subclasses or extreme cases of a continuous distribution, it is necessary to study in detail intermediate cases such as the broad-lined SN 2002ap (Gal-Yam et al. 2002; Foley et al. 2003), which had an intermediate explosion energy ($E_{51} = 4 - 10$; Mazzali et al. 2002) and was not connected with a GRB, or the broad-lined, low energy ($E_{51} \approx 2$) SN 2006aj associated with XRF 060218 (Mazzali et al. 2006, 2007; Maeda et al. 2007).

Here we discuss the case of SN 2003jd, a broad-lined object showing clear evidence of an asymmetric explosion (Mazzali et al. 2005) but with no confirmed GRB connection (Ofek et al. 2003; Hurley et al. 2003). Asymmetry is probably a key factor in understanding the diversity of SNe Ic.

SN 2003jd was discovered (Burket et al 2003) on 2003 Oct. 25 (UT dates are used throughout this paper) with the Katzman Automatic Imaging Telescope (KAIT) during the Lick Observatory Supernova Search (Filippenko et al. 2001; Filippenko 2005). It is located at $\alpha = 23^h21^m03^s.38$ and $\delta =$-04°53′45″.5 (equinox J2000), which is 8.3″ E and 7.7″ S of the centre of the Sb spiral galaxy MCG-01-59-21 (van den Bergh et al. 2005).
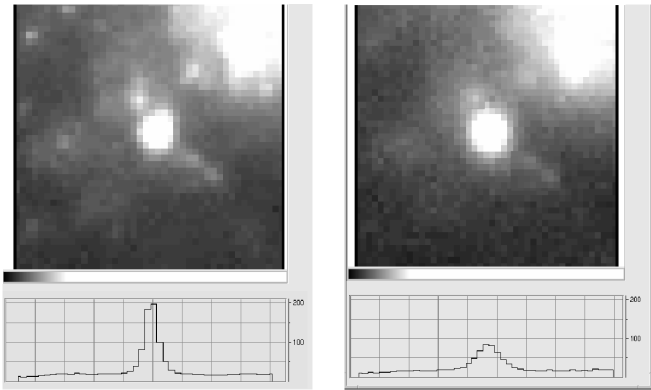
The SN was not visible on 16 Oct. in a KAIT unfiltered

Figure 2. The SN 2003jd region: **a** : *R*-band VLT image (2004 Nov. 15, +382 d after *B* maximum); **b** : *R*-band Subaru image (2005 Dec. 25, +788 d after *B* maximum) of the star-forming region after SN 2003jd faded away. The objects profiles are shown below the images. The profile on the left shows a double component (the broad component is the star-forming region and the narrow one is the SN), while on the right side only the broad component of the star-forming environment is visible.

image (mag < 19), which sets a tight limit to the explosion epoch ($\leqslant$ 13 d before *B* maximum). On 28 Oct., SN 2003jd was classified as a peculiar Type Ic event with very broad features analogous to those of SN 1998bw and SN 2002ap (Filippenko et al. 2003).

The new interest in this kind of event prompted an intensive follow-up campaign at different observing sites, lasting for about three months. Few more observations in the late nebular phase were taken about one year later.

This paper, which presents and discusses these observations, is organized as follows. In §2 we describe the observations and data-reduction techniques. We describe the photometric and spectroscopic data of SN 2003jd in §3 and §4. In §5 we characterize the host galaxy, and in §6 we compare SN 2003jd with a sample of well-studied SNe Ic: 1994I, 1998bw, 2002ap, 2004aw and 2006aj. §7 presents the bolometric light curve of SN 2003jd, computed using all available photometric data. The similarity with SN 2006aj/GRB 060218 is discussed in §8, together with a discussion of the (lack of) evidence for an associated GRB. Finally, in §9, using simple bolometric light-curve modelling, we derive some basic explosion parameters.

2 OBSERVATIONS AND DATA REDUCTION

An extended spectrophotometric monitoring campaign on SN 2003jd started 3 d before *B* maximum and continued through 90 d after *B* maximum, using several telescopes. Additionally, three observations at 10-12 months after explosion were obtained using the 10 m Keck I telescope, the Subaru 8.2 m telescope, and the 8.2 m Very Large Telescope (VLT). The late-time VLT imaging of the SN obtained under very good seeing conditions ($0.5''$) shows a broader component underlying the stellar point spread function (PSF) of the SN, probably owing to contamination from a star-forming region (see Fig. 2).

All photometric and spectroscopic data were pre-

Table 1. Optical photometry of SN 2003jd reference stars[a]

Id	B	V	R	I
1	15.98 (0.01)	15.38 (0.01)	14.99 (0.01)	14.60 (0.01)
2	16.17 (0.01)	15.26 (0.01)	14.73 (0.01)	14.23 (0.01)
3	17.86 (0.02)	17.18 (0.02)	16.76 (0.02)	16.43 (0.02)
4	16.70 (0.02)	15.98 (0.01)	15.53 (0.01)	15.08 (0.01)
5	18.15 (0.02)	17.37 (0.02)	16.87 (0.01)	16.56 (0.02)
6	18.23 (0.01)	16.71 (0.01)	15.70 (0.01)	14.44 (0.01)
7	15.61 (0.02)	14.99 (0.01)	14.61 (0.02)	14.23 (0.02)
8	13.90 (0.01)	13.15 (0.01)	12.75 (0.01)	12.34 (0.01)
9	18.35 (0.03)	17.58 (0.01)	17.08 (0.02)	16.85 (0.02)

[a] The uncertainties are the standard deviation of the mean of the selected measurements.

reduced (trimming, bias subtraction, flat-fielding) using IRAF[1] packages.

In images where the SN was bright, the SN magnitudes were measured using a PSF-fitting technique in the SNOOPY[2] package. At nebular epochs (phase $\geqslant$ 70 d), the magnitudes were measured after subtracting a template image obtained with the Subaru telescope, 788 d after *B* maximum. For the image subtraction we used the ISIS package (Alard 2000), which allows proper matching of the PSF of the target and template images. The template-subtraction technique is an highly effective method to remove background contamination and allows one to measure objects significantly fainter than the background.

Even though we didn't use the template subtraction technique at early phases, a few tests of galaxy subtraction at selected earlier epochs have confirmed that the PSF-fitting technique gives consistent measurements when the SN is bright (deviations < 3%).

Observations of standard fields (Landolt 1992) during photometric nights were used to match a local sequence of reference stars (see Fig. 1 and Tab. 1), which were used to calibrate the observations obtained under non-photometric conditions.

Despite the moderate redshift of SN 2003jd ($z = 0.0187$), the K-correction for the SN photometry are not negligible. We estimated their values by measuring the difference between synthetic photometry in the observed and rest-frame SN spectra (see below). K-corrections between 0.01 and 0.1 mag were measured depending on the band and the SN phase.

Spectroscopic observations were pre-reduced in the same manner as for imaging, with the additional step of fringing contamination removal using the normalized quartz standard. In the extraction of the spectra we took special care to minimize the background contamination subtracting the spectrum of the underlying star-forming region as observed after the SN faded, two years after the explosion. Even so, the Hα, Hβ, [O III], [N II], and [S II] emission lines

from the H II region could not be removed completely. Fortunately, these narrow lines are well distinguished from the broad features of the SN.

All spectra were wavelength and flux calibrated using arc lamps and spectrophotometric standard-star spectra observed during the same night. In most cases observations were obtained with the slit oriented along the parallactic angle (Filippenko 1982). The spectra were also corrected for atmospheric extinction and telluric bands were removed using standard-star observations. The calibrated spectra were compared with the photometry and, when necessary, multiplied by a constant to correct for slit losses.

3   PHOTOMETRY

The $BVRI$ data range from -3 d to 90 d from B maximum with dense coverage and only a small temporal gap (3–11 d past B maximum; see Tab. 2). We also obtained two very late observations which were used to measure the slope of the radioactive-decay tail. In Tab. 2 we report the $BVRI$ magnitude of SN 2003jd in the standard Johnson-Cousins system and the estimated K correction.

The light curves of SN 2003jd in the different bands are shown in Fig. 3. The data up to 85 d after B maximum were obtained mainly through automated follow-up observations with the KAIT, Wise, and Palomar telescopes. Unfortunately, the exposure times used for these observations were independent of the atmospheric conditions and object brightness. This results in a low signal to noise ratio (S/N < 15) for the SN images near 80 d past B maximum. In those exposures where the SN was below the detection limit, we placed upper limits (see Tab.2).

The maximum luminosity[3] occurred on 2003 Oct. 30 at 16.34 ± 0.06 mag in the B band, and 2, 3, and 5 d later in the V, R, and I bands, respectively (Tab. 3). The epoch of explosion is likely shortly before the pre-discovery image taken 13 d before B maximum. Indeed, 13 d is even the rise time suggested by spectral modelling (Sauer et al. in prep.). This rise time is longer than that of SN 2006aj (9.5 d as measured from the date time of the GRB Campana et al. 2006) and smaller than in the case of SN 1998bw (~ 15 d Mazzali et al. 2001). The light curves are typical of SNe Ib/c, with a rapid decline after maximum followed by a much slower decline. The transition, which is not well defined in the case of SN 2003jd, occurs ~ 30 d after B maximum.

Fig. 4 shows the late-time light curves of SN 2003jd, from 50 d to 383 d after B maximum. The short horizontal segments on the right mark the magnitudes of the background star-forming region as measured via PSF fitting on the Subaru images of 2005 Dec. 25 (seeing $\sim 0.8''$). The actual background contamination depends on the sky conditions and is, of course, larger in nights with poor seeing.

The late-time luminosity decline rates were computed via weighted linear least-squares fits to the observations (see Fig. 4 and Tab. 3). The slopes are steeper in all bands than those expected when the energy source is ^{56}Co $\to$ ^{56}Fe decay and the trapping of γ-rays is complete [0.98 mag (100 d)$^{-1}$].

Figure 3. Light curves of SN 2003jd during the photospheric phase, ranging from -3 to 90 d from B maximum. The error bars are computed taking into account both the uncertainty of the PSF fitting of the SN magnitude and the uncertainty due to the background contamination (computed by an artificial-star experiment).
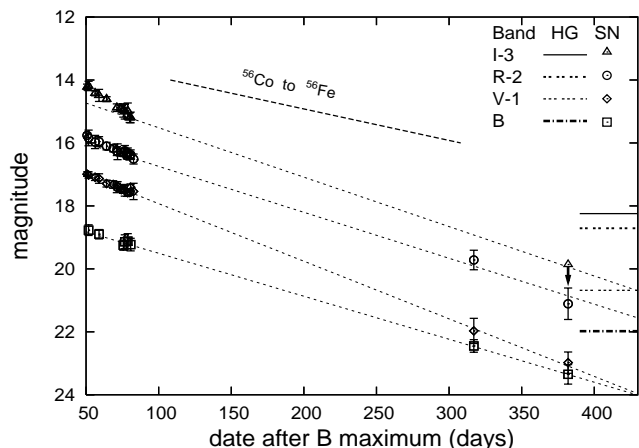
Figure 4. Late-time light curves of SN 2003jd, ranging from 50 to $\sim$400 d past B maximum. The horizontal lines on the right mark the magnitude of the background region.

Adopting the distance modulus of the host galaxy MCG-01-59-21 (μ = 34.46 mag; see §5) and assuming $E(B - V)$ = 0.14 mag for the total interstellar extinction (§5), we estimate that SN 2003jd reached an absolute magnitude at maximum of -18.9 ± 0.3 in the V band. This value is comparable to the magnitude of SN 1998bw (-19.12 ± 0.05)[4] and much brighter than the magnitudes of SN 2002ap (-17.37 ± 0.05) and SN 1994I (-17.5 ± 0.3).

4   SPECTROSCOPY

Spectroscopic monitoring started one day before B maximum light and continued until 51 d after B maximum (see Tab. 4). In addition, using the Subaru and Keck telescopes,

---

[3] Here and generally elsewhere in this paper, the maximum magnitude is computed via a weighted least-squares polynomial fit to the observations.
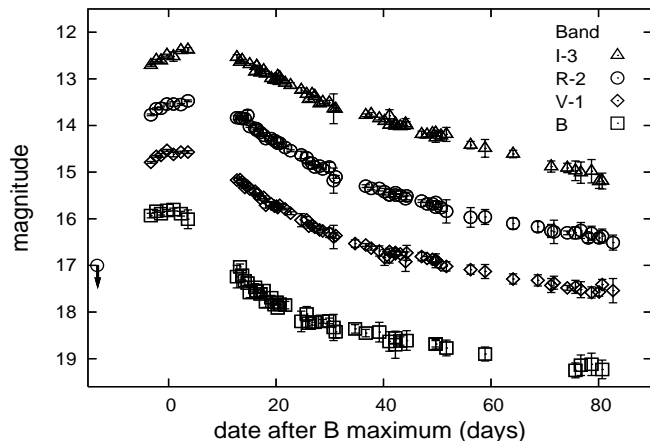
[4] See Tab. 6 for references.

Table 2. Optical photometry of SN 2003jd[a]

UT Date	JD − 2,400,000	Phase[b]	B	$K_{BB}{}^c$	V	$K_{VV}{}^c$	R	$K_{RR}{}^c$	I	$K_{II}{}^c$	Source[d]
16/10/03	52928.70	−13.		−		−	19.0	08		−	0,1
26/10/03	52938.72	−3.2	16.48 (05)	02	16.24 (23)	05	16.15 (02)	08	15.91 (03)	00	1
27/10/03	52939.73	−2.2	16.39 (02)	01	16.12 (24)	05	16.02 (02)	08	15.80 (02)	00	1
28/10/03	52940.65	−1.3	16.43 (04)	01	16.10 (04)	05	16.01 (03)	08	15.81 (04)	00	1
29/10/03	52941.70	−0.3	16.35 (02)	00	15.98 (02)	04	15.92 (02)	07	15.68 (02)	00	1
30/10/03	52942.91	0.9	16.33 (03)	00	16.06 (05)	04	15.91 (05)	07	15.71 (10)	00	7
31/10/03	52944.38	2.4	16.41 (05)	−01	16.01 (02)	03	15.93 (02)	07	15.59 (02)	00	2
02/11/03	52945.69	3.7	16.53 (20)	−02	16.00 (03)	02	15.84 (03)	07	15.58 (06)	00	1
11/11/03	52954.74	12.7	17.73 (25)	−05	16.56 (05)	−01	16.19 (05)	06	15.71 (06)	−02	1
11/11/03	52955.34	13.3	17.61 (07)	−05	16.55 (03)	−02	16.20 (04)	06	15.82 (02)	−01	2
12/11/03	52955.74	13.7	17.82 (10)	−05	16.72 (03)	−02	16.31 (08)	05		−	2
12/11/03	52956.24	14.2	17.69 (10)	−05	16.60 (06)	−02	16.20 (03)	05	15.78 (03)	−01	1
13/11/03	52956.74	14.7	17.86 (04)	−05	16.68 (03)	−02	16.24 (11)	05		−	1
13/11/03	52957.17	15.1	17.96 (12)	−05	16.75 (02)	−02	16.38 (03)	05	15.88 (03)	−01	2
14/11/03	52958.17	16.1	17.95 (08)	−05	16.79 (06)	−02	16.41 (07)	05	16.03 (06)	−01	2
14/11/03	52958.44	16.4	18.03 (03)	−05	16.85 (02)	−02	16.42 (02)	05	15.91 (02)	−01	9
14/11/03	52958.44	16.4	18.03 (03)	−05	16.85 (02)	−02	16.45 (02)	05	15.91 (02)	−01	9
15/11/03	52959.18	17.1	18.10 (10)	−05	16.93 (05)	−03	16.50 (09)	05	16.05 (06)	−02	2
16/11/03	52959.74	17.7	18.02 (06)	−05	16.92 (03)	−03	16.56 (03)	05	16.00 (02)	−02	1
16/11/03	52960.18	18.1	18.26 (12)	−05	17.09 (07)	−03	16.63 (07)	05	16.07 (06)	−02	2
17/11/03	52961.18	19.1	18.17 (05)	−05	17.06 (05)	−03	16.63 (05)	05	16.16 (10)	−02	2
18/11/03	52961.74	19.7	18.32 (12)	−05	17.11 (08)	−03	16.67 (08)	05	16.20 (08)	−02	1
18/11/03	52962.17	20.1	18.27 (06)	−05	17.10 (02)	−03	16.70 (10)	05	16.19 (10)	−02	2
18/11/03	52962.35	20.3	18.39 (06)	−05	17.13 (04)	−03	16.73 (02)	05	16.11 (02)	−02	8
19/11/03	52962.74	20.7	18.32 (09)	−05	17.08 (04)	−03	16.73 (03)	05	16.14 (03)	−02	1
20/11/03	52963.74	21.7	18.33 (08)	−05	17.16 (02)	−03	16.82 (02)	04	16.26 (03)	−02	1
21/11/03	52964.74	22.7		−	17.25 (04)	−03	16.89 (02)	04	16.31 (07)	−03	1
23/11/03	52966.74	24.7	18.68 (23)	−05	17.40 (14)	−04	16.97 (08)	04	16.41 (05)	−03	1
24/11/03	52967.74	25.7	18.52 (16)	−05	17.38 (07)	−04	17.04 (11)	04	16.49 (07)	−03	1
24/11/03	52968.17	26.1	18.73 (08)	−05	17.52 (04)	−04	17.15 (04)	04	16.60 (05)	−03	2
25/11/03	52968.74	26.7	18.71 (07)	−05	17.51 (04)	−04	17.15 (05)	04	16.49 (05)	−03	1
25/11/03	52969.22	27.2	18.71 (13)	−05	17.55 (03)	−04	17.23 (03)	04	16.53 (03)	−03	2
26/11/03	52970.17	28.1		−	17.61 (03)	−04	17.22 (04)	04	16.69 (06)	−04	2
27/11/03	52970.74	28.7	18.69 (05)	−04	17.63 (04)	−03	17.27 (03)	04	16.66 (03)	−04	1
28/11/03	52971.93	29.9	18.68 (06)	−04	17.67 (10)	−03	17.22 (10)	04	16.66 (05)	−04	7
29/11/03	52972.74	30.7	18.82 (28)	−04	17.76 (26)	−03	17.42 (27)	03	16.79 (32)	−04	1
29/11/03	52973.18	31.1	18.91 (14)	−04	17.73 (06)	−03	17.44 (03)	03	16.80 (04)	−04	2
03/12/03	52976.74	34.7	18.85 (10)	−04	17.90 (08)	−03		−		−	1
05/12/03	52978.74	36.7	18.95 (08)	−03	17.94 (04)	−02	17.63 (03)	03	16.92 (03)	−05	6
06/12/03	52979.74	37.7		−	18.01 (05)	−02	17.68 (04)	03	16.90 (04)	−06	6
07/12/03	52981.27	39.2	18.93 (22)	−03	18.08 (12)	−02	17.68 (05)	03	16.98 (03)	−06	2
08/12/03	52982.27	40.2		−	18.12 (17)	−02	17.75 (08)	03	17.05 (07)	−06	2
09/12/03	52983.19	41.1	19.13 (21)	−03	18.09 (08)	−01	17.81 (05)	03	17.12 (07)	−06	2
09/12/03	52983.19	41.1		−	18.22 (12)	−01	17.81 (06)	03	16.92 (13)	−06	6
10/12/03	52984.22	42.2	19.05 (12)	−03	18.14 (05)	−01	17.77 (04)	02	17.09 (04)	−06	6
10/12/03	52984.22	42.2	19.20 (29)	−03	18.12 (06)	−01	17.82 (03)	02	17.14 (04)	−06	2
11/12/03	52985.17	43.1	19.12 (10)	−03	18.15 (04)	−01	17.83 (04)	02	17.15 (05)	−07	2
12/12/03	52986.19	44.1		−	18.32 (21)	−01	17.90 (06)	02	17.09 (11)	−07	2
13/12/03	52986.32	44.3	19.11 (21)	−03	18.13 (16)	−01	17.83 (08)	02	17.12 (08)	−07	8
15/12/03	52989.19	47.1		−	18.22 (10)	00	17.94 (04)	02	17.31 (08)	−07	2
16/12/03	52990.18	48.1		−	18.25 (05)	00	18.00 (03)	02	17.31 (04)	−08	2
17/12/03	52991.17	49.1		−	18.28 (06)	00	18.00 (06)	02	17.29 (03)	−08	2
17/12/03	52991.74	49.7	19.19 (10)	−03	18.29 (07)	00	17.97 (05)	02	17.28 (07)	−08	1
17/12/03	52991.74	49.7	19.18 (07)	−03	18.31 (16)	00	18.07 (05)	02	17.37 (10)	−08	6
18/12/03	52992.74	50.7		−	18.40 (08)	01	18.08 (09)	02	17.33 (10)	−08	6
19/12/03	52993.74	51.7	19.26 (17)	−04	18.43 (10)	01	18.16 (25)	02	17.30 (16)	−08	1
24/12/03	52998.28	56.2		−	18.51 (11)	01	18.28 (21)	01	17.54 (08)	−08	2
27/12/03	53000.94	58.9	19.39 (15)	−04	18.55 (15)	01	18.27 (16)	01	17.59 (19)	−09	7
01/01/04	53006.17	64.1		−	18.71 (11)	01	18.41 (12)	00	17.72 (08)	−09	2
06/01/04	53010.74	68.7	>19.2	−05	18.73 (12)	01	18.47 (11)	00	>17.7	−09	1
08/01/04	53013.21	71.2		−	18.84 (15)	00	18.56 (14)	00	17.98 (12)	−10	2

Table 2 continued

UT Date	JD − 2,400,000	Phase[b]	B	K_{BB}[c]	V	K_{VV}[c]	R	K_{RR}[c]	I	K_{II}[c]	Source[d]
09/01/04	53013.74	71.7		–	18.77 (15)	00	18.58 (25)	00		–	1
11/01/04	53016.21	74.2		–	18.89 (05)	00	18.60 (05)	−01	18.01 (11)	−10	2
13/01/04	53017.74	75.7	19.73 (17)	−05	18.86 (15)	00	18.60 (13)	−01	18.07 (21)	−09	1
14/01/04	53018.74	76.7	19.62 (22)	−05	18.92 (17)	−01	18.54 (17)	−01	18.11 (23)	−09	1
15/01/04	53020.19	78.1		–		–	18.70 (10)	−01		–	2
16/01/04	53020.74	78.7	19.60 (24)	−05	18.97 (12)	−01	18.60 (16)	−01	18.08 (26)	−09	1
17/01/04	53022.19	80.1			18.96 (09)	−01	18.70 (11)	−01	18.31 (16)	−09	2
17/01/04	53022.74	80.7	19.72 (21)	−04	18.80 (11)	−01	18.66 (16)	−01	18.30 (17)	−09	1
19/01/04	53024.74	82.7	>19.3	−04	18.93 (27)	−01	18.81 (17)	−01	>18.1	−09	1
22/01/04	53027.18	85.1		–		–	>18.4	−01	>18.5	−09	2
26/01/04	53031.18	89.1		–		–	>18.2	−01		–	2
11/09/04	53259.10	317.1	23.00 (21)	01		–	21.92 (31)	00		–	3
11/09/04	53259.10	317.1		–	23.38 (40)	00		–		–	3[e]
15/11/04	53324.02	382.	23.90 (31)	01	24.38 (35)	−01	23.61 (50)	00	>23.0	00	4
25/12/05	53730.1	788	21.6		21.3		20.6		21.2		3[f]

[a] The errors (in parentheses, in decimal) are computed taking into account both the uncertainty of the PSF fitting of the SN magnitude and the uncertainty due to the background contamination (computed by the artificial-star experiment).
[b] Relative to the B maximum (JD = 2,452,942.0).
[c] K correction (in decimal).
[d] 0 = IAU Circular 8232.
  1 = 0.76 m Katzman Automatic Imaging Telescope, Lick Observatory, Mt. Hamilton, CA (USA).
  2 = 1 m Telescope, Wise Observatory, Negev desert, Mitzpe Ramon (Israel).
  3 = 8.2 m Subaru Telescope, National Astr. Obs. of Japan, Mauna Kea (Hawaii).
  4 = 8.2 m ESO-VLT Telescope, Paranal Observatory, Atacama (Chile).
  5 = 3.5 m Telescopio Nazionale Galileo, La Palma, Canary Isl. (Spain).
  6 = 1.5 m Telescope, Palomar Observatory, Mt. Palomar, CA (USA).
  7 = 2.3 m Advanced Technology Telescope, Siding Spring Observatory, Coonabarabran (Australia).
  8 = 1.82 m Copernico Telescope, INAF - Osservatorio di Asiago, Mt. Ekar, Asiago (Italy).
[e] Synthetic photometry from spectrum.
[f] Lower limit for the magnitude of the star-forming region at the position of the SN, measured with aperture photometry in a circle of radius 0.5″.

Table 3. Main parameters for light curves of SN 2003jd

Parameter	B	V	R	I
Date of max (JD −2,400,000)	52942.0 ± 1 (2003 Oct. 30)	52944.1 ± 1	52944.7 ± 1	52947.2 ± 1
Apparent magnitude at max	15.75 ± 0.24	15.49 ± 0.18	15.48 ± 0.15	15.36 ± 0.13
Absolute magnitude at max	−18.7 ± 0.3	−18.9 ± 0.3	−19.0 ± 0.2	−19.1 ± 0.2
Late-time decline γ (mag d^{-1})	0.0141 ± 0.0013	0.0189 ± 0.0005	0.0149 ± 0.003	> 0.016
Phase range	75–382	71–382	71–382	71–382

we secured two spectra at late epochs, 317 and 354 d after B maximum, respectively.

4.1 Photospheric spectra

The spectra obtained in the first two months after explosion are shown in Fig. 5 (upper panel; wavelengths are in the SN rest frame). The early-time spectra show broad absorption features similar to those observed in SNe 1998bw, 2002ap, and 2006aj. These features suggest that a significant amount of the gas is moving at velocities larger than 15000 km s^{-1}.

As the spectra evolve and the velocity at which they form decreases, the spectral features become less blended than in SN 1998bw and the typical features of normal SNe Ic emerge, even if the spectral time evolution remains slower than that of SN 1994I (see §7.1).

The absorption features close to 5660 Å and 6200 Å are probably due to Na I D and Si II, respectively, with possible contamination by He I in the Na I D feature and Ne I in the Si II. Contamination by Hα or C II to the Si II line can also not be excluded. The Ca II near-infrared (IR) triplet and O I at 7770 Å are prominent and only marginally blended.

Close to ∼6770 Å and ∼7005 Å, SN 2003jd shows two not easily identified lines. Helium at ∼11,000 km s^{-1} could explain these features, but the complete absence of the He I 6678 Å and the low strength of the feature at ∼5650 Å, that in this case should be identified as He I at 5876 Å, make this identification unlikely.

In Fig. 6 we show the spectrum of SN 2003jd ∼ 2 weeks past maximum, compared with the spectra of other SNe Ic at similar epochs.

The spectra are arranged in order of increasing line

Table 4. Journal of spectroscopic observations

UT Date	JD − 2,400,000	Phase[a] (days)	Range (Å)	Resolution FWHM[b] (Å)	Equipment[c]
2003 Oct 28	52940.5	−1	3200–10000	7	Shane+Kast
2003 Oct 28	52940.6	−1	3750–7550	7	FLWO+FAST+300gpm
2003 Oct 29	52941.7	0	3700–7550	7	FLWO+FAST+300gpm
2003 Oct 30	52942.9	+1	3720–7550	7	FLWO+FAST+300gpm
2003 Oct 30	52943.4	+1	3500–7500	25	Ekar+AFOSC+gm.4
2003 Oct 31	52944.4	+2	3720–7550	7	FLWO+FAST+300gpm
2003 Nov 01	52945.0	+3	3720–7550	7	FLWO+FAST+300gpm
2003 Nov 04	52948.0	+6	3500–7500	25	Ekar+AFOSC+gm.4
2003 Nov 15	52959.4	+17	3200–10250	12	TNG+DOLORES+gm.LRB,LRR
2003 Nov 18	52962.2	+20	3500–10100	25	Ekar+AFOSC+gm.2,4
2003 Nov 19	52963.3	+21	3720–7500	7	FLWO+FAST+300gpm
2003 Nov 20	52963.9	+22	3720–7550	7	FLWO+FAST+300gpm
2003 Nov 20	52964.3	+22	3500–7800	25	Ekar+AFOSC+gm.4
2003 Nov 21	52964.7	+23	3720–7550	7	FLWO+FAST+300gpm
2003 Nov 22	52965.5	+24	3720–7550	7	FLWO+FAST+300gpm
2003 Nov 23	52966.5	+25	3200–10000	7	Shane+Kast
2003 Nov 23	52966.7	+25	3720–7550	7	FLWO+FAST+300gpm
2003 Nov 24	52967.8	+26	3720–7550	7	FLWO+FAST+300gpm
2003 Nov 27	52970.9	+29	3720–7550	7	FLWO+FAST+300gpm
2003 Nov 28	52971.8	+30	3720–7550	7	FLWO+FAST+300gpm
2003 Nov 28	52972.3	+30	3500–9200	6	ATT+DBS+gm.300B
2003 Nov 29	52973.5	+31	3200–10000	7	Shane+Kast
2003 Dec 04	52977.7	+36	3720–7550	7	FLWO+FAST+300gpm
2003 Dec 19	52992.7	+51	3600–8820	7	FLWO+FAST+300gpm
2004 Sept 11	53259.1	+317	3100–9350	10	Subaru+FOCAS+B300+Y47
2004 Oct 18	53296.1	+354	3100–9350	8	Keck+LRIS
2005 Dec 25	53730.2	+788 [d]	3100–7200	10	Subaru+FOCAS+B300+Y47

[a] Relative to the B-band maximum light (JD = 2,452,942.0).

[b] FWHM of night-sky emission lines

[c] Ekar = 1.82 m Copernico Telescope, INAF - Osservatorio di Asiago, Mt. Ekar, Asiago (Italy).
TNG = 3.5 m Telescopio Nazionale Galileo, La Palma, Canary Isl. (Spain).
Subaru = 8.2 m Subaru Telescope, National Astr. Obs. of Japan, Mauna Kea, Hawaii (USA).
Keck = 10 m Keck I Telescope, W. M. Keck Obs., Mauna Kea, Hawaii (USA).
ATT = 2.3 m Advanced Technology Telescope, Siding Spring Observatory, Coonabarabran (Australia).
FLWO = 1.5 m Telescope, Fred Lawrence Whipple Observatory, Mt. Hopkins, Arizona (USA).
Shane = Shane 3-m telescope at Lick Observatory, Mt. Hamilton, CA (USA).

[d] Spectrum of the SN site 26 month after explosion.

width (top to bottom), as exemplified by the iron lines around 4000–5000 Å. In particular, the two absorptions with minima at ∼4720 and ∼4990 Å , caused by the Fe II lines (4924 Å, 5018 Å, 5170 Å), are clearly visible in the SN 1994I-like SNe Ic, while they are partially or completely blended in the other objects.

The increase of the line width is also visible in the red part of the spectra, with feature such as O I 7774 Å and the Ca II near-IR triplet.

4.2 Photospheric velocity

Because of severe line blending in broad-lined SNe Ic, estimating of the photospheric velocity from direct measurement of the minimum of specific spectral absorption lines is particularly difficult.

We used the Si II line (6355 Å) as the best tracer of the photospheric velocity, with the caveat that other ions may contribute to the ∼6200 Å absorption. In SN 1994I,
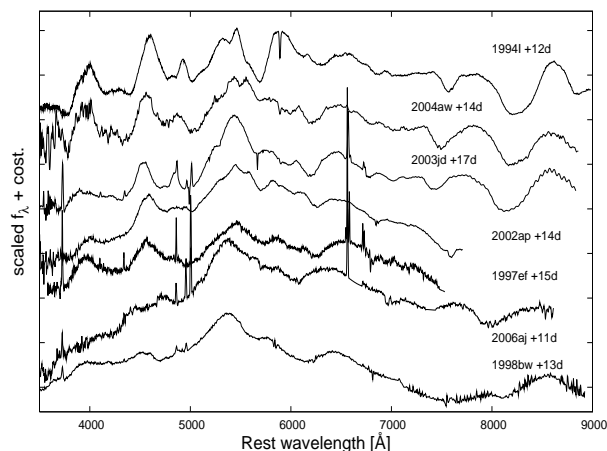

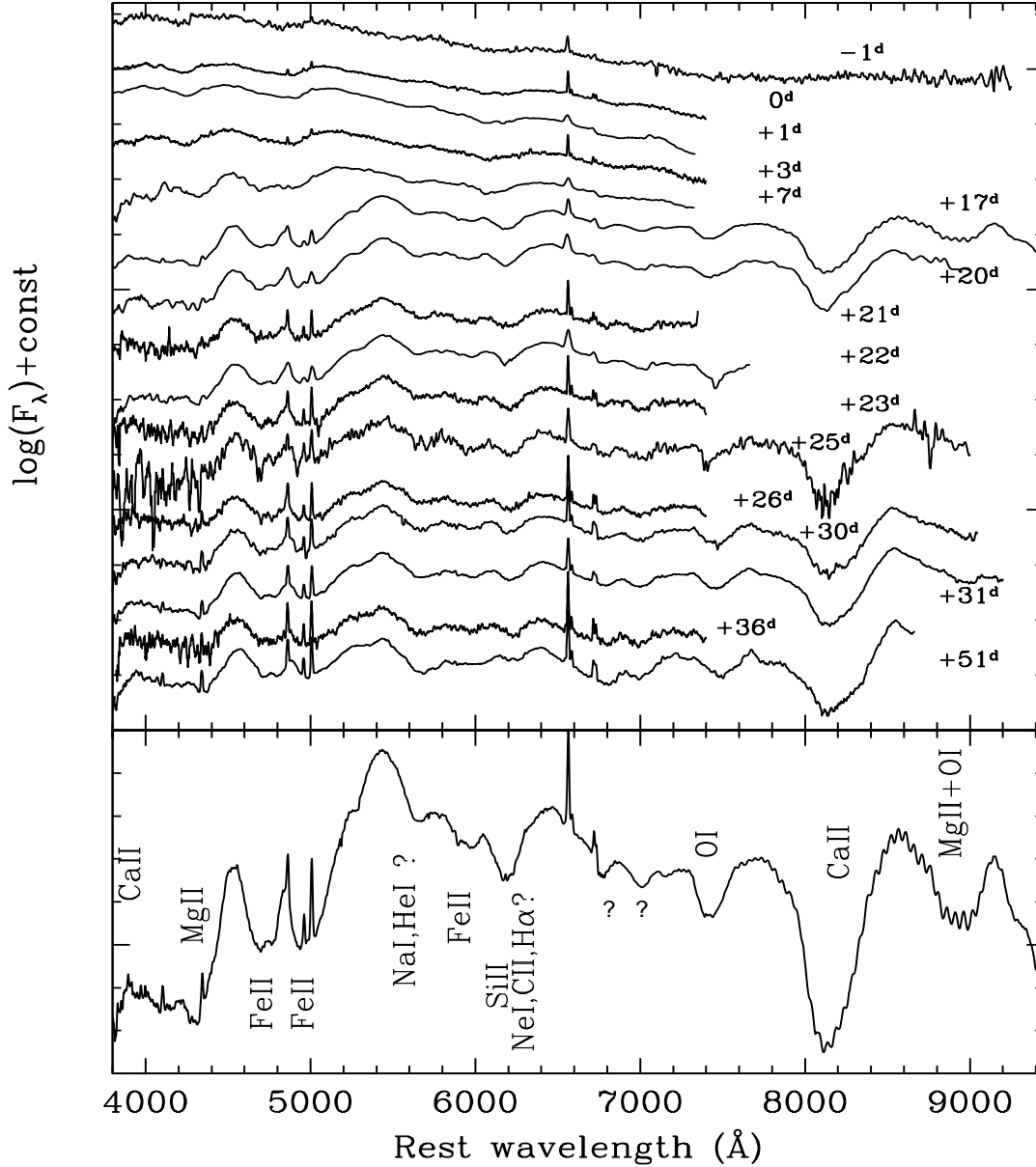**Figure 6.** Comparison spectra of SNe Ic at ∼2 weeks past *B* maximum.

Figure 5. (Top) Spectroscopic evolution of SN 2003jd from −1 d to +51 d with respect to *B* maximum light. The wavelength scale is in the supernova rest frame. The spectra are smoothed over a window of 10 Å. The narrow lines are host-galaxy contamination. (Bottom) Identification of the main features in the +17 d spectrum. The following lines are marked: Ca II (H&K, 8498 Å, 8542 Å, 8662 Å); O I (7774 Å); Fe II (4440 Å, 4555 Å, 4924 Å, 5018 Å, 5170 Å); He I (5876 Å) and Na I D (5890 Å, 5896 Å); Mg II (4481 Å). The feature near 6100 Å is mainly attributed to Si II (6355 Å), contaminated by another feature, probably Ne I, but contamination by C II or Hα cannot be excluded. The feature near 5650 Å is most likely due to the Na I D. Contamination by He I (5876 Å) cannot be excluded but would imply a unusually low velocity for the He I layer.

for example, a number of potential contaminants have been suggested: detached He I (6678 Å) (Clocchiatti et al. 1996), detached C II (6580 Å) (Elmhamdi et al. 2006), detached Hα (Branch et al. 2006), and Ne I (6402 Å) (Sauer et al. 2006).

In Fig. 7, we show a comparison of the Si II spec-

tral region for three SNe Ic (1994I, 2003jd, and 1996aq), all showing a second component in the ∼6200 Å absorption line indicative of line blending.

As in the case of SN 1994I, we assume that for SN 2003jd only the blue component is due to Si II, whereas the red wing is dominated by some other lines. With this as-
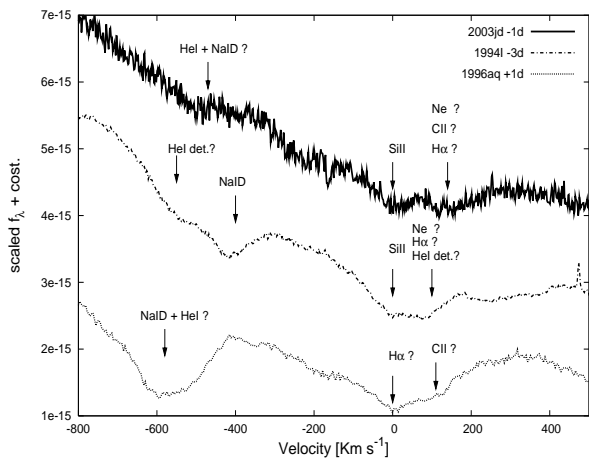
Figure 7. Spectral comparison SN 2003jd, SN 1994I, and SN 1996aq in the range between Na I D and Si II. The zero point of the abscissa is placed at the blue component of the line at ~6200 Å (rest frame). All of the spectra show a double-dipped or relatively flat-bottomed profile, probably due to more than one component. The line identifications were proposed by Clocchiatti et al. (1996), Elmhamdi et al. (2006), Branch et al. (1996), and Sauer et al. (2006) for SN 1994I, and by Elmhamdi et al. (2006) for type Ib/c SN 1996aq.

sumption we estimate a photospheric velocity of ~14,200 $km\,s^{-1}$ at B maximum and ~7900 $km\,s^{-1}$ one month later. These values are in good agreement with the photospheric velocity deduced from spectral modelling ($v \approx 13{,}500\ km\,s^{-1}$ and $v \approx 8000\ km\,s^{-1}$, respectively; Sauer et al. in prep.).

The identification of the second contributor to this feature remains dubious: Ne I is a possible candidate, but C II or Hα cannot be excluded as suggested for other SNe Ic (Branch et al. 2006).

The evolution with time of the expansion velocities measured from a few of the features mentioned above is shown in Fig. 8. The O I and Ca II velocities are significantly higher than the Si II velocities, but with similar slopes. On the other hand, the velocity of Na I D shows a very rapid decline near B maximum. This is probably not real, but rather due to contamination by He I.

4.3   Late-phase spectra and asymmetry

The nebular spectra (see also Mazzali et al. 2005) show forbidden emission lines, in particular Mg I] and [O I], typical of SNe Ic, but with a peculiar double-peak profile (see Fig. 9). Mazzali et al. (2005) interpreted this as evidence for a strongly asymmetric explosion with some of the material moving at high velocity within a jet-like structure. The double-peak profile suggests an angle of $\geqslant 70°$ between the jet axis and the line of sight. This configuration is consistent with the non-detection of an associated GRB, because the GRB would be beamed along the jet direction and not towards the observer (see §8).

Recently more SN Ib/c with a double peak have been found (Maeda et al. submitted). Here we show another SN Ib/c, namely SN 1996aq, showing a double-peak [O I] emission line similar to that of SN 2003jd (see Fig. 9). While a detailed analysis of the observations has not yet been performed, we note that SN 1996aq appears to be
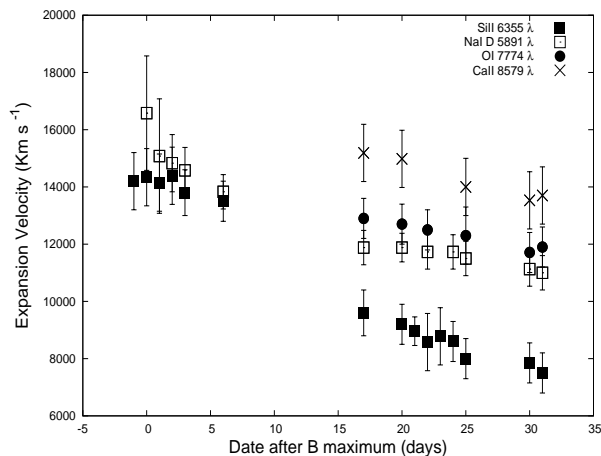

Figure 8. Photospheric velocity for the Na I D (5890 Å, 5896 Å), Si II (6355 Å), O I (7770 Å), and Ca II (8498 Å, 8542 Å, 8662 Å). The measurements of the O I velocity were done fitting a Gaussian to the absorption minimum. The fitting of the Si II line was done using two Gaussian functions, taking the blue one as the Si II line. The photospheric velocity of Ca II and Na I D were calculated at the blueshift of the minimum away from an estimated wavelength of 8579 Å (Ca II) and 5891 Å (Na I D) via a weighted average of the three and two components of Ca II and Na I D, respectively (Thomas et al. 2004).
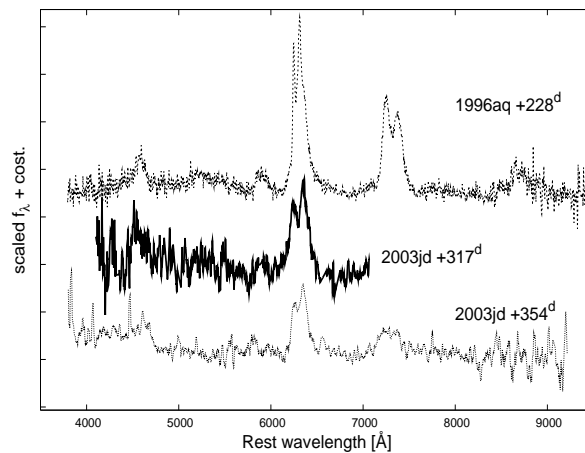

Figure 9. Nebular spectra of SN 2003jd (317 d, 354 d) and SN 1996aq (228 d).

a typical SN Ic with a moderate photospheric expansion velocity (9000 $km\,s^{-1}$, as deduced from spectral modelling (Elmhamdi et al. 2006)) and luminosity ($M_V \approx -17$ mag). This would suggest that asymmetric explosions are not unique to energetic broad-line SNe Ic.

5   ENVIRONMENT PROPERTIES: MGC-01-59-021

There are no direct estimates of the distance to MGC-01-59-21, the host galaxy of SN 2003jd, and therefore we must resort to the recession velocity and the Hubble law. However, this method gives a good estimate of the distance, albeit with a large uncertainty.

Table 5. Main parameters for SN 2003jd and its host galaxy

Parent galaxy	MCG-01-59-021
Galaxy type	Sb pec[a]
RA (2000)	$23^h21^m03^s.38$
Dec (2000)	$-04°53'45.5''$
Recession velocity [km s^{-1}]	5625[b]
Distance modulus ($H_0 = 72$)	34.46 ± 0.20 mag
$E(B-V)_{host}$	$0.10^{+0.10}_{-0.05}$ mag[c]
$E(B-V)_{Gal}$	0.044 mag[d]
Offset from nucleus	8.3'' E, 7.7'' N

[a] van den Bergh et al. 2005.
[b] LEDA, corrected for Local Group infall (208 km s^{-1}).
[c] Calculated from the equivalent width of the Na I D lines (Turatto et al. 2003).
[d] Schlegel et al. (1998).

Using the radial velocity corrected for Local Group infall into the Virgo Cluster (5625 km s^{-1}; LEDA) and a Hubble constant of 72 ± 5 km s^{-1} Mpc^{-1} (Freedman et al. 2001; Spergel et al. 2003), we derive a distance modulus $\mu = 34.46 \pm 0.20$ mag. The error include the uncertainty in the Hubble constant and an uncertainty of 200 km s^{-1} for the radial velocity of MGC-01-59-021 owing to peculiar motions.

The Galactic extinction in the direction of SN 2003jd reported by Schlegel et al. (1998) is $E(B-V)_{Gal} = 0.044$ mag.

The presence in the spectra of a narrow Na I D line at the host-galaxy redshift with equivalent width EW = 0.62 ± 0.02 Å support extinction in the host galaxy. Interstellar gas is usually associated with dust, and indeed there is a general correlation between Na I D EW and colour excess, although with a large dispersion (Turatto et al. 2003).

Since SN 2003jd at B-band maximum was already one of the bluest SNe Ic ever observed (see Fig. 11), we exclude the possibility that the relation between Na I D EW and colour excess for SN 2003jd can follow the steeper relation of Turatto et al. (2003). Assuming a conservative relation reported by Turatto et al. (2003), namely $E(B-V) = 0.16$EW, we estimate $E(B-V)_{host} \approx 0.10^{+0.10}_{-0.05}$ mag, where the uncertainty accounts for the dispersion in the correlation. The total reddening suffered by SN 2003jd is $E(B-V) \approx 0.14^{+0.10}_{-0.05}$, where the uncertainty in the Galactic component is negligible.

The spectra of the host galaxy taken at +788 d, long after the fading of the SN, can be used to estimate the metallicity and star-formation rate (SFR) of the region were SN 2003jd exploded. Following Pettini & Pagel (2004), from the [O III] and [N II] line strengths we derive an oxygen abundance of $12 + \log(O/H) = 8.4 \pm 0.1$ dex. A slightly higher value ($12 + \log(O/H) = 8.7 \pm 0.1$ dex) is obtained using the R_{23} index ((([O III] + [O II])/Hβ) of Pagel et al. (1979). The two estimates bracket the measurement by Modjaz et al. (2007); they confirm that the metallicity of the SN 2003jd host is below average for local galaxies and similar to that of the SN 1998bw host (Modjaz et al. 2007). On the other hand, MCG-01-59-021 is a luminous galaxy, $M_B = -20.3$ mag (LEDA), which is somewhat at odds with the medium to low metallicity (see Fig. 5 of Modjaz et al. 2007, and Fig. 1 of Prieto et al 2007).

The SFR at the SN location can be estimated from the Hα flux, 7.1 ± 0.5 erg s^{-1} cm^{-2}. Following Kennicutt (1998), we estimate a SFR ≈ 0.04 M$_\odot$ yr^{-1}, which is in fair agreement with the value derived by Modjaz et al. (2007) (SFR = 0.07 M$_\odot$ yr^{-1}). This SFR is typical for H II regions, and similar for instance to that derived for the environment of SN 2006aj: SFR ≈ 0.06 M$_\odot$ yr^{-1} (Pian et al. 2006).

6 LIGHT AND COLOUR CURVES OF SN 2003JD

In Fig. 10 the B, V, R, and I light curves of SN 2003jd are compared with those of a sample of the best-observed SNe Ic spanning a range of observed properties, from the *normal* SN 1994I to the very energetic SN 1998bw, including intermediate objects like SNe 2002ap, 2006aj, and 2004aw. For comparison, the light curves are normalized to their maximum brightness in each band.

The light curves of SN 2003jd agree well with those of SNe 2002ap and 2006aj, especially in the V and R bands. SN 1998bw and SN 2004aw appear to be much slower than SN 2003jd, while SN 1994I is the other extreme.

From a comparison of the $B - V$ colour curves (Fig. 11) it appears that the colour at maximum, $B - V = 0.2$ mag, is actually $\sim$0.1–0.2 mag bluer than that of all other events. SN 2003jd evolves rapidly in colour reaching a redder colour $B - V = 1.05$ mag in about 20 d, which is between SN 1998bw ($B - V = 1.0$ mag) and SNe 2002ap and 2004aw ($B - V = 1.15$ mag). SN 1994I evolves rapidly in color but remains always bluer ($B - V = 0.9$ mag at $\sim$10 d), whereas SN 2006aj reaches a much redder colour ($B - V = 1.6$ mag at $\sim$15 d).

After the peak, the colour turns slowly back to the blue, following the evolution of SNe 1998bw and 2002ap, while SN 2004aw remains red. This behavior could be real or simply due to an underestimate of the reddening of SN 2004aw, as suggested by Benetti et al. (2006). For SN 2004aw we have adopted the colour excess computed by Taubenberger et al. (2006), $E(B-V) = 0.37$ mag, using the conservative relation between reddening and the EW of the interstellar Na I D lines (Turatto et al. 2003).

6.1 Light-curve parameters

In an attempt to characterize quantitatively the light curves of SNe Ic, by analogy with SNe Ia we use four observable parameters: (i) the absolute magnitude at maximum brightness (M); (ii) the "stretch" factor (s) relative to the light curves of SN 1998bw which is taken as reference[5] (Perlmutter et al. 1997; Bloom et al. 2002); (iii) the difference in V-band magnitude between maximum and +60 d, after expanding the time scale using the stretch factor ($\Delta m_{60}s$); and (iv) the slope of the linear late-time tail (γ).

As shown in Fig. 12, the stretch factor allows an excellent description of the light curves of different objects up to $\sim$30 d after maximum, whereas some spread remains at later phases. The parameter $\Delta m_{60}s$ has been introduced to

---

[5] Perlmutter et al. (1997) introduced the quantity s for SNe Ia; it is used to expand or contract linearly the time scale of a light curve in order to match a template.
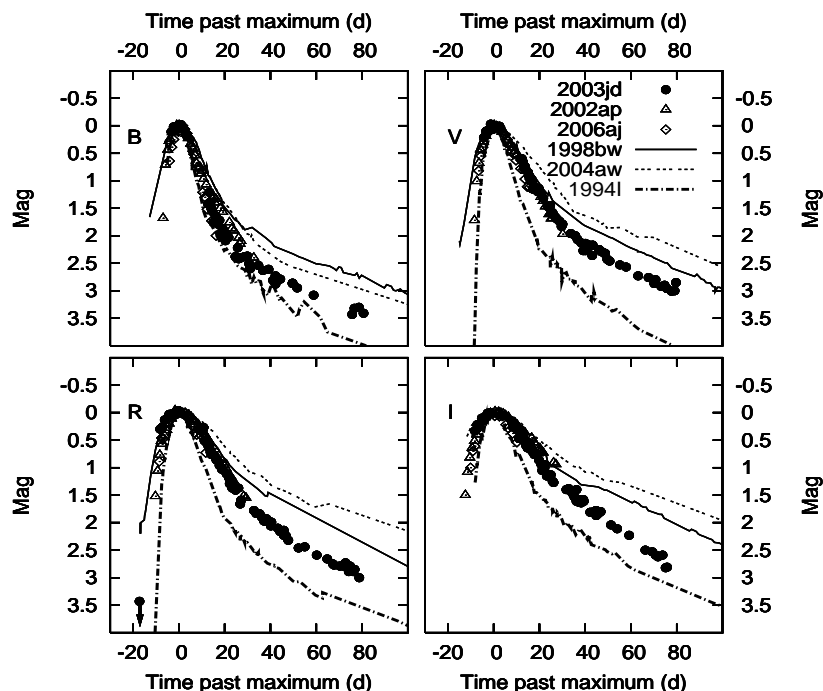
Figure 10. Comparison among light curves of different SNe Ic. The magnitude and the phase have been shifted to coincide at maximum brightness in each band.
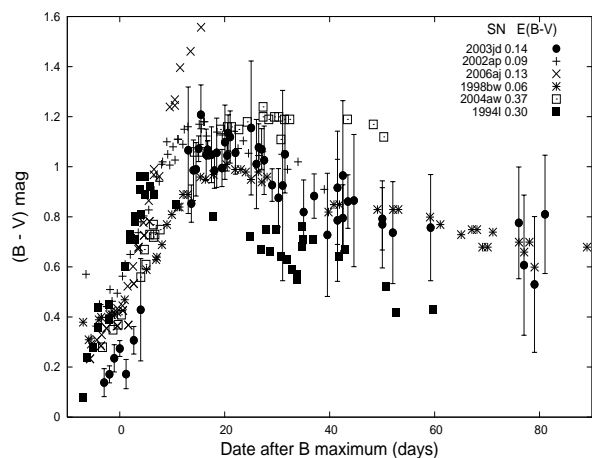

Figure 11. Comparison of the intrinsic colour curves of different SNe Ic. While among SNe Ia the colour at ∼30 d is quite similar, SNe Ic show a large scatter. We used the $E(B-V)$ value from Tab. 6
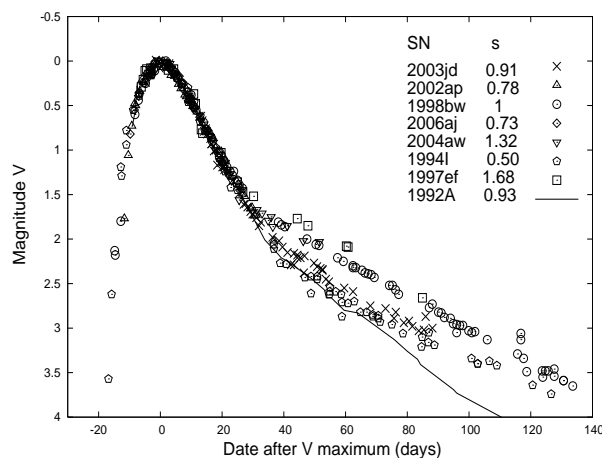

Figure 12. Comparison of V-band light curves of different SNe Ic corrected for stretch factor. SN 1998bw is the reference object with stretch factor defined to equal 1. The light curves are scaled in magnitude and phase to the V maximum

take this spread into account. In Fig. 12, we also show the V-band light curves of SN 1997ef and SN 1992A. SN 1997ef is the SN Ic with the slowest known light curve, even slower than that of SN Ic 2004aw, while SN 1992A is a SN Ia. Up to +30 d the stretched V-band light curve of SN 1992A follows the same shape, but later it has a steeper tail than SNe Ic. This is due to the inefficient trapping of γ-rays in SNe Ia than in SNe Ic. At wavelengths longer than the V band (not shown here), the light-curve shapes of SNe Ia and SNe Ic are distinguished by the second peak that SNe Ia show at ∼2 weeks after B maximum.

Whether a correlation between stretch and luminosity applies to SNe Ic as it does for SN Ia should be investigated.

However the uncertainties on the reddening estimate and the small number of SNe Ib/c with good data coverage[6] make the issue complex (Valenti et al. in prep.).

The values of various parameters for SN 2003jd and other SNe Ic are reported in Tab. 6.

Our analysis confirms that SN 2003jd is an intermediate case as far as luminosity evolution is concerned, similar to SNe 2002ap and 2006aj; the most extreme objects are SN

---

[6] to estimate the stretch factor some photometric data in the pre-maximum phase are necessary
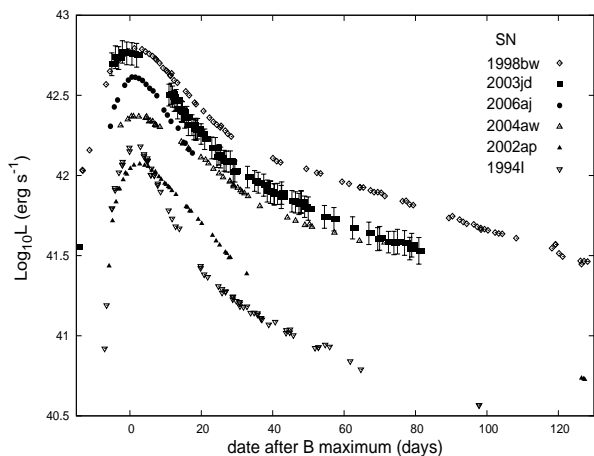
Figure 13. Quasi-bolometric ($BVRI$) light curves of SN 2003jd and other SNe Ic. We assume $H_0 = 72$ km s^{-1} Mpc^{-1}. Extinctions and distance moduli are given in Tab. 6.

1997ef, which appears to have the slowest light curves, and SN 1994I, which is the fastest.

7   BOLOMETRIC LIGHT CURVE OF SN 2003JD

The bolometric light curve is a fundamental observational description of a supernova, which can be readily used to validate model predictions. Unfortunately, because of the restricted spectral range covered by the observations, in general it is impossible to derive true bolometric luminosities for SNe. Moreover, the light curve in a given photometric band can be heavily affected by the evolution of few individual lines and does not reflect the bolometric evolution of the SN. As a first-order approximation to the bolometric luminosity, it is possible to integrate the SN emission in the spectral window accessible from the ground, redwards of the ultraviolet (UV) atmospheric cutoff to the near-IR (JHK). This is known as the *uvoir* bolometric luminosity.

In the case of SN 2003jd we have to face the additional limitation that observations are available only for the $BVRI$ optical bands. To cope with this limitation, we adopt the following strategy: (i) we integrate the $BVRI$ emission of SN 2003jd as a function of time (the "quasi-bolometric light curve"); (ii) we compare the results with the same quantity derived for other SNe Ic; and (iii) we attempt to estimate the expected contribution from the unavailable UV and IR bands.

To derive the $BVRI$ integrated SN luminosity, the observed magnitudes were corrected for reddening, converted to the flux density at the effective wavelength using the definition of the standard Johnson-Cousins system (Buser & Kurucz 1978; Bessell 1983), and integrated using Simpson's rule. Adopting a distance modulus for each SN, the integrated flux was then converted to luminosity.

The comparison between quasi-bolometric ($BVRI$) light curves (Fig. 13) confirms that as far as light-curve shape is concerned, SN 2003jd is most similar to SNe 2006aj and 2002ap, though the latter is significantly less luminous. Even though SN 1998bw is the most similar to SN 2003jd
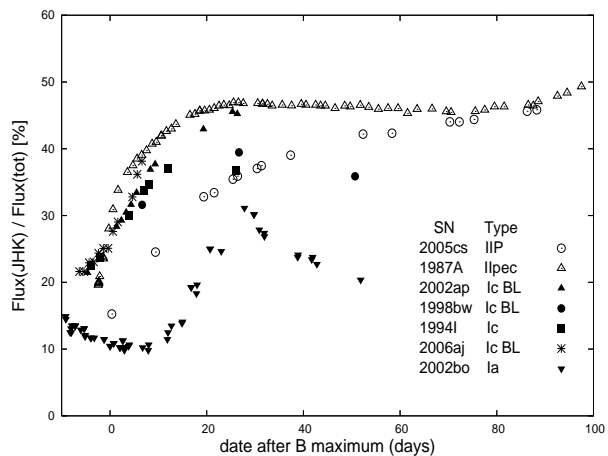

Figure 14. IR contribution to the total flux: SNe II (open symbols), and SNe Ia and SNe Ic (filled symbols). The IR and optical fluxes of SN 1994I are measured from synthetic spectra (Sauer et al. 2006), The optical and IR fluxes of the other SNe are computed integrating the photospheric data, (*uvoir* for the total flux, and *uvoir* minus $UBVRI$ for the IR flux): SN 2005cs (Pastorello et al. 2006;   Pastorello et al. in prep.), SN 2002ap (Foley et al. 2003; Yoshii et al. 2003), SN 1998bw (Galama et al. 1998; Patat et al. 2001), and SN 2002bo (Benetti et al. 2005; Krisciunas et al. 2004).

in absolute brightness, the light curve evolves more slowly than that of SN 2003jd. The similarity of SN 2003jd with SN 2006aj/XRF 060218 extends to other properties, as we discuss in the following sections.

To estimate the contribution of the missing UV and IR spectral regions to the bolometric luminosity, we must resort to comparisons with other SNe. For this purpose we computed the contribution of JHK emission to the total flux for different SNe Ic and, for comparison, for two SNe II and for a SN Ia (Fig. 14). The IR contribution is indeed significant, increasing from 20% near maximum brightness up to 40–50% one month later. This is similar to other core-collapse SNe, and larger than in SNe Ia, where it reaches $\sim$ 30% one month past B maximum and decreases to 20% at late phases. Conversely, the UV contribution for SNe Ib/c and SNe Ia is not so important: $\sim$15% during the first week after explosion, decreasing later to only 5–10%.

Because of the similarity with the quasi-bolometric light curve of SN 2002ap[7], we assume that the fractional contributions of the UV and IR emission to the bolometric light curve of SN 2003jd are the same as for SN 2002ap[8].

We added this contribution to the quasi-bolometric ($BVRI$) light curve and we used the derived bolometric light curve of SN 2003jd to estimate the peak bolometric luminosity, the slope of the late-time tail and moreover to compute a rough estimate of the physical parameters: M_{ej}, M_{Ni}, and E_k (see §9).

---

[7] Even though the light-curve shape of SN 2003jd is similar to that of both SN 2006aj and SN 2002ap, the JHK data coverage of SN 2002ap is larger than that of SN 2006aj.
[8] Since the stretch factors of SN 2002ap ($s = 0.78$) and SN 2003jd ($s = 0.91$) are similar, the UV and IR contributions to the bolometric light curve of SN 2003jd are included without using the stretch factor as a temporal stretch.
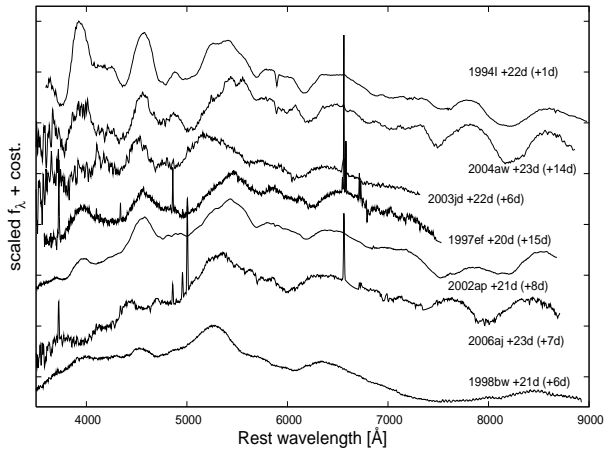
Figure 15. Comparison of spectra of SNe Ic at a stretched time of ∼3 weeks past explosion (computing time in SN 1998bw frame). Next to each object name, we report the phase after the explosion in the stretched time scale, and, in parentheses, the phase relative to the observed B maximum.

Figure 16. Comparison of spectra of SNe Ic at a stretched-time of ∼5 weeks past explosion (computing time in SN 1998bw frame). Next to each object name, we report the phase after the explosion in the stretched time scale and, in parentheses, the phase relative to the observed B maximum.

The spectrum of SN 2006aj is missing, because the object was too close to the Sun at the relevant time.

The peak bolometric magnitude of SN 2003jd ($M_{bol} = -18.65 \pm 0.20$ mag) is nearly as bright as that of SN 1998bw ($M_{bol} = -18.76 \pm 0.11$ mag), but the light curve of SN 2003jd declines more steeply after maximum. The slope of the late-time tail (from 70 to 400 d) is $\gamma = 0.015 \pm 0.001$ mag d^{-1}. This is similar to that of SN 1998bw and implies a progressively increasing transparency to the γ-rays produced in the ^{56}Co $\rightarrow$ ^{56}Fe radioactive decay.

7.1 Spectral evolution and stretch factor

In §6 we introduced the stretch factor, to take into account the different time evolution of SN Ic light curves. The spectral evolution seems to follow a similar behavior: SN 1997ef, which has the slowest light curve in our sample, still shows photospheric features at 150 d (Mazzali et al. 2004), while SN 1994I, which has the fastest light curve, starts to show nebular features just two months after maximum brightness.

In order to investigate whether this behavior is a signature of a spectral sequence, we compared spectra of SNe Ic using a stretched time scale. In practice, we took as reference the inferred epoch of explosion for each event (see Tab. 7), and we labeled spectra with a "stretched" phase obtained by scaling the phase past explosion by the stretch factor derived from the light-curve shape.

We then compared spectra of different objects at the same stretched time. This is shown in Figs. 15 and 16, where the epochs are ∼3 weeks and ∼5 weeks past explosion, respectively, in the time frame SN 1998bw.

As the figures show, with this approach part of the spread of the sample is removed. SN 1994I, with the fastest light curves (SN 1994I, $s = 0.50$) and SN 2004aw, with the second-slowest light curves (SN 2004aw, $s = 1.32$), appear very similar both in their line profiles and expansion velocities. The major differences between the two SNe seen close to 5700–5800 Å in Fig. 6, disappears in Fig. 15. Indeed, the strong absorption close to 5700–5800 Å in SN 1994I at +2 weeks (mainly caused by Na I D) develops at about +1 month in SN 2004aw (see Fig. 16).
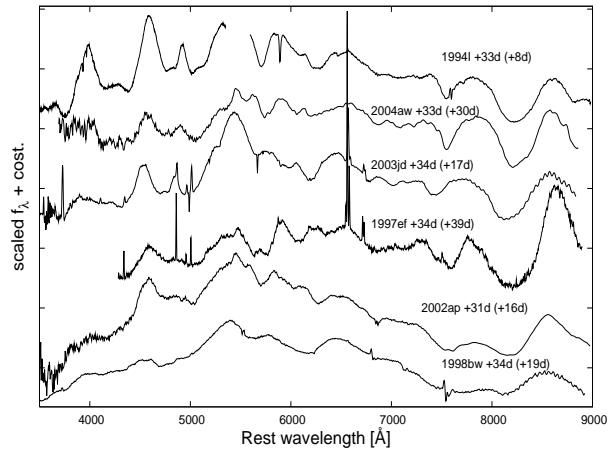
The stretch of the time scale does not completely remove the heterogeneity of the sample. Indeed, SNe 2002ap, 2006aj, and 2003jd show broad lines at all epochs, but never as broad as in SN 1998bw. The features of SN 1994I and SN 2004aw are the narrowest of the sample. While the time stretching for the light curves works well, for spectroscopy it can partially help in the comparison of similar objects (SN 2004aw and SN 1994I).

Other parameters are required to explain the remaining differences. The different line widths are probably connected to the expansion velocity and to the kinetic energy per ejected mass ratio (E_k/M_{ej}). Moreover, the asymmetric explosion and the viewing angle make the scenario even more complex, as is already the case for nebular spectra (Maeda et al. 2006a) and light curves (Maeda et al. 2006b)

The flux deficiency in the blue part of the spectra seen in the figures for a few SNe Ic deserves some discussion. Mazzali et al. (2002) suggested that the blue deficiency is related to the high expansion velocity and to the consequent severe blending of the many Fe II lines at these wavelengths.

The fact that SN 2003jd has higher blue emission than SNe 1998bw and 2006aj, and a relatively narrow Fe feature at ∼4900 Å, strongly suggests that the Fe layers have slower expansion velocities in SN 2003jd than in other objects. In a scenario where iron is mainly expelled along the jet (Maeda et al. 2002), the lower expansion velocity of the Fe lines in SN 2003jd is in agreement with the idea that in this SN, the jet was out of the line of sight (Mazzali et al. 2005).

However, except the blue excess, the object with spectra similar to those of SN 2003jd is SN 2006aj. This is visible in Figs. 6 and 15, and it is also evident comparing the spectra close to maximum brightness (see Fig. 17).

Table 6. Parameters of the optical light curves of SNe Ic[a]

SN	stretch V	Magnitude B	Magnitude V	Magnitude R	Magnitude I	γ_V (mag d^{-1})	$\Delta m_{60}s$ V (mag)	References for the data[b]
1994I	0.50 ⟨0.02⟩	−17.1 ⟨0.3⟩	−17.5 ⟨0.3⟩	−17.7 ⟨0.2⟩	−17.54 ⟨0.12⟩	0.0184 ⟨0.0005⟩	2.67 ⟨0.04⟩	R96
2006aj	0.73 ⟨0.02⟩	−18.15 ⟨0.10⟩	−18.67 ⟨0.08⟩	−18.81 ⟨0.06⟩	−18.96 ⟨0.05⟩	–	–	S06;P06;M06
2002ap	0.78 ⟨0.01⟩	−16.79 ⟨0.07⟩	−17.37 ⟨0.05⟩	−17.41 ⟨0.04⟩	−17.33 ⟨0.04⟩	0.0203 ⟨0.0003⟩ 0.015 ⟨0.002⟩[c]	2.5 ⟨0.2⟩	Y03;F03;P03
2003jd	0.91 ⟨0.09⟩	−18.7 ⟨0.3⟩	−18.9 ⟨0.3⟩	−19.0 ⟨0.2⟩	−19.1 ⟨0.2⟩	0.0189 ⟨0.0005⟩	2.53 ⟨0.13⟩	This work
1998bw	1	−18.65 ⟨0.07⟩	−19.12 ⟨0.05⟩	−19.14 ⟨0.04⟩	−19.04 ⟨0.04⟩	0.0181 ⟨0.0004⟩	2.23 ⟨0.05⟩	G98;P01
2004aw	1.32 ⟨0.13⟩	−17.7 ⟨0.4⟩	−18.0 ⟨0.3⟩	−18.1 ⟨0.3⟩	−18.2 ⟨0.2⟩	0.017 ⟨0.006⟩	–	T06
1997ef	1.68 ⟨0.10⟩	–	−17.1 ⟨0.2⟩	–	–	0.013 ⟨0.002⟩	2.02 ⟨0.13⟩	M04

[a] The extinctions, the distance moduli, and the data used for the SNe Ic are as follows. SN 2002ap: $E(B-V) = 0.09$ mag (Yoshii et al. 2003), $\mu = 29.46$ mag (Sharina et al. 1996); SN 2004aw: $E(B-V) = 0.37$ mag, $\mu = 34.17$ mag (Taubenberger et al. 2006); SN 1998bw: $E(B-V) = 0.06$ mag, $\mu = 32.76$ mag (Patat et al. 2001); SN 1994I: $E(B-V) = 0.3$ mag, $\mu = 29.60$ mag (Sauer et al. 2006); SN 2006aj: $E(B-V) = 0.13$ mag, $\mu = 35.6$ mag (Pian et al. 2006); SN 1997ef: $E(B-V) = 0.04$ mag, $\mu = 33.5$ mag (Iwamoto et al. 2000); and SN 2003jd: $E(B-V) = 0.14$ mag, $\mu = 34.46$ mag (this work).
[b] R96 = Richmond et al. (1996); S06 = Sollerman et al. (2006); P06 = Pian et al. (2006); M06 = Mirabal et al. (2006); Y03 = Yoshii et al. (2003); F03 = Foley et al. (2003); P03 = Pandey et al. (2003); P01 = Patat et al. (2001); G98 = Galama et al. (1998); T06 = Taubenberger et al. (2006); I00 = Iwamoto et al. (2000); M04 = Mazzali et al. (2004).
[c] SN 2002ap shows an inflection point at $t \approx 250$ d. The slope is measured in two different temporal ranges: 70–250 d and 250–400 d.
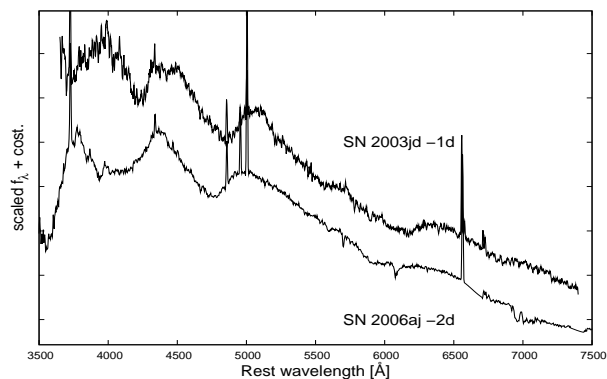
Figure 17. Comparison of spectra of SN 2003jd and SN 2006aj close to B maximum.

8   WAS THERE A GRB ASSOCIATED WITH SN 2003JD?

The close similarity of SN 2003jd with SN 2006aj/XRF 060218 prompted the quest for a possible GRB associated with SN 2003jd.

The main argument against a relativistic jet along or off from the line of sight is the non-detection of SN 2003jd at radio wavelengths, despite the extensive search for radio emission extending from soon after explosion to 1.6 yr later (Soderberg et al. 2006). The early radio observations are sensitive to both typical GRBs and sub-energetic GRBs (e.g., XRF-SN 2006aj) viewed along the jet axis, while at late times, since the ejecta are roughly spherical, radio observations should be sensitive to both typical GRBs and sub-energetic GRBs viewed off-axis.

For SN 2003jd, the earliest radio upper limit (at $t \approx$ 10 d) implies a radio luminosity a factor of 10 below that of a sub-energetic GRB radio afterglow such as XRF-SN 2006aj (Soderberg et al. 2006), at a comparable epoch. Therefore, radio and X-ray observations show no evidence for any typical GRB or a sub-energetic GRB viewed along the axis.

On the other hand, the double-peaked [O I] emission in the nebular spectra suggests significant asymmetry of the explosion, consistent with the presence of a jet-like structure oriented away from the line of sight. Even though there was no late-time radio of SN 2003jd, suggesting no evidence for a typical GRB viewed off-axis (Soderberg et al. 2006), an off-axis GRB in a low-density circumstellar medium cannot be excluded.

We investigated the (lack of) evidence for a possible GRB associated to SN2003jd (Ofek et al. 2003; Hurley et al. 2003). Assuming that the GRB was simultaneous with the SN, the temporal window to be searched is well defined (16± 2 Oct. 2003; Sauer et al. in prep.).

To search for a possible GRB associated with SN 2003jd, we used the data of the interplanetary network (IPN). In the 14–18 Oct. 2003 search window, the IPN consisted of the HETE and RHESSI spacecraft in low-Earth orbit, INTEGRAL (SPI-ACS detector) at 0.5 light-seconds from Earth, Wind (Konus detector) at 1.8 light-seconds from Earth, Mars Odyssey (High Energy Neutron Detector and Gamma Sensor Head detectors) at 268 light-seconds from Earth, and Ulysses (GRB experiment) at 2940 light-seconds from Earth. All instruments were on and operating nominally throughout the search window, although Konus-Wind was in a solar particle event, which raised its threshold slightly.

In this configuration, the IPN acts as a true all-sky monitor for GRBs and other fast transients, with virtually no Earth-occultation or duty cycle considerations. Its lower-energy threshold is ∼25 keV, and its flux and fluence thresholds, although very dependent on the burst time history, are ∼1 photon cm^{-2} s^{-1} and 10^{-6} erg cm^{-2}, respectively. At these levels, the probability of detecting a burst is roughly 50%. Bursts with fluxes and fluences an order of magnitude below these values can be detected, but with probabilities of 30–40%. The IPN has observed and detected the SN-associated GRBs 980425 (SN 1998bw), 021211 (SN 2002lt), 030329 (SN 2003dh), and 031203 (SN 2003lw). It did not detect XRF 060218 (SN 2006aj), probably because the spectrum of this event was too soft.

Three GRBs were clearly detected in the search window by more than one spacecraft. All of them can therefore be classified as confirmed cosmic events, and could be localized. However, the localization regions excluded the position of SN 2003jd in all cases. Other, weaker events may also have been present, particularly in the Konus-Wind data, but their interpretation is complicated by the solar particle background.

Thus, if SN 2003jd indeed produced a GRB, we are left with the following possible conclusions: (i) the GRB was beamed away from us; (ii) the GRB was weak, below the IPN flux and fluence thresholds; or (iii) the GRB had a soft spectrum, with little or no emission above 25 keV. Any combination of the above properties is also possible.

9 PHYSICAL PARAMETERS FROM THE BOLOMETRIC LIGHT CURVE

The modelling of the bolometric light curve can be used to constrain the parameters of the explosion, in particular M_{ej}, M_{Ni}, and E_k. For this purpose, the SN luminosity evolution can be divided into two phases according to the different dominating physical processes.

• *Photospheric Phase* ($t \leqslant 30$ d past explosion): We adopt the simple analytical model developed by Arnett (1982) for SNe Ia, which is well suited also for core-collapse SNe lacking a hydrogen recombination phase (SNe Ib/c). The model assumes homologous expansion of the ejecta, spherical symmetry, and that all radioactive Ni is located in the centre. It adopts a constant optical opacity k_{opt}, a small initial radius before explosion ($R_0 \to 0$), and the diffusion approximation for photons (i.e., the ejecta are optically thick; see App. A). With respect to Arnett (1982), we include also the energy produced by the $^{56}\text{Co} \to ^{56}\text{Fe}$ decay, not only the energy produced by the $^{56}\text{Ni} \to ^{56}\text{Co}$ decay.

• *Nebular Phase* ($t \geqslant 60$ d past explosion): At late phases, with the decrease of the optical depth of the ejecta, the emitted luminosity is directly related to the instantaneous amount of energy deposition by the γ-rays from the ^{56}Co decay, by the γ-rays coming from the electron-positron annihilation, and by the kinetic energy of the positrons (cf. Sutherland et al. 1984; Cappellaro et al. 1997).

In the transition phase ($30 \leqslant t \leqslant 60$ d), where the ejecta are not completely thick but also not sufficiently thin, both approximations fail. This portion of the light curve was ignored during the fit.

The dominant physical effect to consider is that in SNe Ic, as in SNe Ia, the ejecta become rapidly and progressively more transparent to γ-rays, which thus escape. This is accounted for by multiplying the decay energy by an absorption probability (for the γ-ray photons) and by an annihilation probability (for the positrons). In the assumption of homologous expansion, these probabilities decline with time.

While this simple model gives good fits to the overall light curves of SNe Ia (Arnett 1982, see appendix A), for SNe Ic we found an inconsistency between the parameters derived from the fitting of the early and late-time light curves. In particular, the rapid evolution of the light curve of the photospheric phase requires a high transparency of
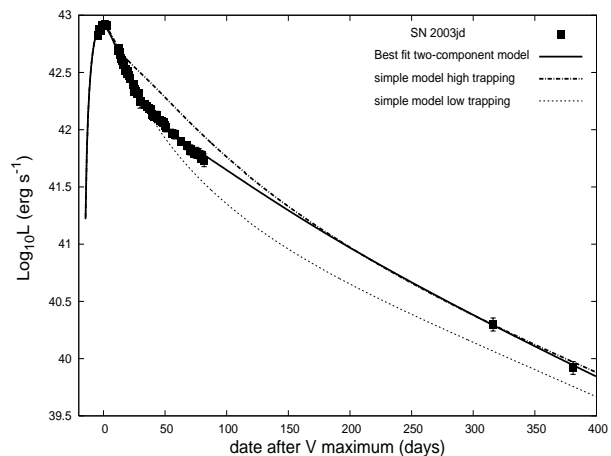

Figure 18. Light-curve fit with simple models (low and high γ-ray trapping; dotted and dot-dashed lines, respectively) and with a two-component model (solid line) of the bolometric light curve of SN 2003jd. While the simple models cannot fit the photospheric phase and the nebular phase in a consistent way, the two-component model account for the light curve in both phase.

γ-rays (see Fig. 18) which, however, results in too low a predicted luminosity at late phase.

This was already noted by Maeda et al. (2003), who obtained a fair overall fit to the light curves of SNe Ic by schematically dividing the SN ejecta into two regions: a high-density inner region and a low-density outer region with high and low γ-ray trapping, respectively.

It is fair to assume that the luminosities emitted by the two regions sum up to produce the total luminosity when the emission from the inner region is not absorbed by the outer ejecta. This is indeed reasonable in the nebular phase, when the outer layer is basically transparent. Conversely, during the photospheric phase the opposite regime holds: the inner region is optically thick and the emerging luminosity is a small fraction of the total luminosity. Indeed, we found that at the epoch of maximum, for typical fit parameters, the flux emerging from the inner region is at most 15–30% of the total flux.

Using this two-component model increases the number of parameters from 3 to 6, which were finally reduced to 5 assuming a homogeneous distribution of Ni in the inner and outer layers. The 5 parameters are $M_{Ni}(tot)$, $M_{ej}(tot)$, $E_k(inner)$, $E_k(outer)$, and the fraction of the total mass concentrated in the dense, low-velocity inner ejecta.

In addition, the width of the light curve during the photospheric phase (w_{lc}) and its slope in the nebular phase (γ_{lc}) have a similar dependence on M_{ej} and E_k:

$$w_{lc} \propto \frac{M_{ej}^{3/4}}{E_k^{1/4}} \quad \text{and} \quad \gamma_{lc} \propto \frac{M_{ej}}{E_k^{1/2}}. \tag{1}$$

This introduces a degeneracy in the estimate of M_{ej} and E_k which can be removed by using some additional constraint from spectroscopy. More precisely, assuming a homogeneous density of the ejecta, the photospheric velocity at maximum is related to the kinetic energy and the ejected mass through the relation (Arnett 1982)

$$v_{ph} \approx \frac{3}{5} \frac{2E_k}{M_{ej}}. \tag{2}$$

As we mentioned above, at maximum the outer ejecta give the main contribution to the observed luminosity. Hence, assuming a homogeneous density in this region and measuring the photospheric velocity, we constrain the kinetic energy of the outer layers for a given mass, and thus resolve the degeneracy of Eq. 1.

For the photospheric velocity we adopt the values derived from spectral modelling (see Tab 7). Uncertainties are typically of the order of 10% .

The best fit of the bolometric light curve of SN 2003jd is shown in Fig. 18 (thick solid line). The values of the physical parameters derived from the model are $M_{Ni}(tot) = 0.36 \pm 0.04$ M$_\odot$, $M_{ej}(tot) = 3.0^{+0.5}_{-0.5}$ M$_\odot$, and $E_k(tot) = 7^{+3}_{-2} \times E_{51}$. The uncertainty in the nickel mass is mainly due to that in the distance. The uncertainty in the photospheric velocity affects both the uncertainty in M_{ej} and E_k.

The values of M_{ej}, M_{Ni}, and E_k obtained by fitting the light curves of our sample of SNe Ic are reported in Tab.7. For comparison, we give estimates of the same parameters obtained from the spectral and light-curve modelling available in the literature. While the ^{56}Ni and E_K values are consistent with those in literature, the values of M_{ej} are smaller of ~ 30 %. A similar underestimate of the ejected mass, together with an underestimate of the kinetic energy, was found by Richardson et al. (2006) using an analytical light curve model similar to our simple model. The two-components model reproduce better the light curve giving also a better estimate of the kinetic energy. Therefore we considered, to be conservative, an error of 30% in our estimate of the ejected mass of SN 2003jd ($M_{\rm ej} = 3 \pm 1$ M$_\odot$).

This estimate of the ejected mass indicates that the progenitor C+O star had a mass of $\sim$3–7 M$_\odot$, which evolved most likely from a main-sequence star with $M_{\rm ms}$ $\sim$22–28 M$_\odot$.

If the star was on the low side of this range, it is likely to have collapsed to a neutron star. The small remnant mass would than favour the eject ion of a large mass of ^{56}Ni as in SN 2006aj, possibly also via a magnetar. However, the ejecta of SN 2006aj were relatively spherically symmetric (Mazzali et al. 2007), unlike those of SN 2003jd. Although asphericity may be present in most, or possibly all core-collapse SNe, it is not clear that low-energy events can be as highly aspherical as either SN 2003jd or SN 1998bw (Mazzali et al. 2001; Maeda et al. 2002). On the other hand, the morphological similarity between the very aspherical ejecta of SN 2003jd and those of SN 1998bw (Mazzali et al. 2005) is an argument in favour of the collapsar scenario for SN 2003jd as well, in which case the mass of the progenitor would probably have been close to the high side of the range mentioned above.

A large E_k/M_{ej} ratio is required to reproduce the broad features. Indeed, with $E_{51}/M_{ej} \approx 2.3$, SN 2003jd is second only to SN 1998bw ($E_{51}/M_{ej} \approx 4.2$). SN 2004aw has energy comparable to that of SN 2003jd, but a larger ejected mass ($E_{51}/M_{ej} \approx 1.6$). This is the reason for the slower evolution of the light curve, accompanied by narrow lines as in SN 1994I ($E_{51}/M_{ej} \approx 1.3$).

In conclusion, SN 2003jd is a broad-line SN Ic, more massive and more energetic than the broad-line SNe 2006aj and 2002ap, but certainly less massive and energetic than SN 1998bw.

10 SUMMARY

We have presented optical photometry and spectroscopy of SN 2003jd spanning from 3 d before B-band maximum to $\sim$400 d after maximum. SN 2003jd shows the typical spectral features of a SN Ic, but broadened as in the case of SNe 2002ap and 2006aj.

The light curves are similar in shape to those of SNe 2002ap and 2006aj, but the peak luminosity is rather similar to that of SN 1998bw.

The comparison with a sample of well-studied SNe Ic confirms the heterogeneity of this SN class. However, the application of time stretching (as for SNe Ia) helps in homogenizing this class of SNe, reducing the differences among the light curves and facilitating spectral comparisons. Different explosion energies and progenitor masses are likely to be the main reasons for the discrepancies. The different viewing angles from which the SNe are observed (given the evidence for asymmetric explosions) may also explain some of the differences, but this effect is probably not large, at least for the light-curve shape (Maeda et al. 2006b). It may, however, affect the spectra (Tanaka et al. 2007). The E_k/M_{ej} ratio seems to be the main factor in producing broad features.

The similarity to SN 2006aj, the presence of broad features, and the asymmetry shown by the oxygen double peak in the nebular spectra are in favour of an asymmetric explosion oriented away from the line of site. The radio observations argue that the asymmetry did not extended to relativistic velocities, although uncertainties in the CSM mean that 2003jd could still be a mis-directed GRB.

Finally, we used a simple model for the bolometric light curve to obtain the main physical parameters of SN 2003jd. The derived values confirm that SN 2003jd is a broad-line SN similar to SN 2002ap and SN 2006aj, but with a larger ejected mass ($M_{ej} = 3.0 \pm 1.0$ M$_\odot$) and kinetic energy ($E_k(tot) = 7^{+3}_{-2} \times E_{51}$ erg) and producing a large quantity of ^{56}Ni ($M_{Ni} = 0.36 \pm 0.04$ M$_\odot$). Comparing the physical parameters of SN 2003jd with those of other SNe Ic (Nomoto et al. 2007), SN 2003jd appears to represent a link between broad-lined SNe (2002ap and 2006aj) and GRB-associated supernovae (SNe 1997ef, 1998bw, 2003dh, and 2003lw).

Table 7. Physical parameters for SNe Ic derived from models of the bolometric light curves[a]

SN	V_{ph}^a km s^{-1}	T_{exp}^b days	$M_{Ni}(tot)$ M$_\odot$	$M_{ej}(tot)$ M$_\odot$	$E_k(tot)$ 10^{51} erg s^{-1}	$E_k(inner)$ 10^{51} erg s^{-1}	$M_{Ni}(inner)/$ $M_{Ni}(tot)$	$M_{Ni}(*)$ M$_\odot$	$M_{ej}(*)$ M$_\odot$	$E_k(*)$ 10^{51} erg s^{-1}
1994I	11000	11 ± 2	0.065 ± 0.03	$0.7^{+0.3}_{-0.1}$	$0.9^{+0.7}_{-0.1}$	$0.0017^{+0.005}_{-0.001}$	$0.22^{+0.03}_{-0.04}$	~0.07	~0.9	~1
2002ap	14000	8 ± 1	0.073 ± 0.02	$1.6^{+0.5}_{-0.1}$	$2.4^{+2}_{-0.4}$	$0.05^{+0.08}_{-0.01}$	0.40-0.56	~0.1	~2.5	~4
2004aw	14000	~ 15	0.21 ± 0.03	5^{+2}_{-1}	$8^{+8}_{-1.5}$	$0.18^{+0.4}_{-0.13}$	0.38-0.50	–	–	–
2003jd	13500	13 ± 2	0.36 ± 0.04	3.0 ± 0.5	7^{+3}_{-2}	$0.02^{+0.05}_{-0.01}$	0.18-0.28	–	–	–
1998bw	18000	15 ± 1	0.49 ± 0.04	$8^{+0.5}_{-0.1}$	34^{+3}_{-1}	$0.26^{+0.04}_{-0.01}$	$0.29^{+0.01}_{-0.01}$	0.5	10–11	30–60

[a]The $E(B-V)$ values and the distance moduli are reported in Tab. 6. For comparison, we report in the last three columns [labeled with (*)] the values of M_{ej}, M_{Ni}, and E_k, computed with the spectral and light-curve modelling: SN 1998bw and SN 1994I (Nomoto et al. 2001), SN 2002ap (Mazzali et al. 2007), and SN 2004aw (Kawabata et al. in prep.).

[b]V_{ph} is the photospheric velocity close to the maximum of the bolometric light curve.

[c]T_{exp} is the time elapsed from the explosion to the B maximum. The V_{ph} and T_{exp} values are taken from spectral modelling: SN 1998bw (Mazzali et al. 2001), SN 1994I (Sauer et al. 2006), SN 2002ap (Mazzali et al. 2007), SN 2006aj (Mazzali et al. 2006), SN 2004aw (Kawabata et al. in prep.), and SN 2003jd (Sauer et al. in prep.).

der contract NAS 5-26555. A.V.F.'s group at the University of California, Berkeley is supported by National Science Foundation (NSF) grant AST–0607485 and by the TABASGO Foundation. KAIT was made possible by generous donations from Sun Microsystems, Inc., the Hewlett-Packard Company, AutoScope Corporation, Lick Observatory, the NSF, the University of California, and the Sylvia & Jim Katzman Foundation. K. Hurley is grateful for IPN support under the following grants and contracts: JPL 958056 (Ulysses), MIT SC-A-293291 (HETE), NAG5-13080 (RHESSI), NAG5-12614 (INTEGRAL), and NAG5-11451 (HETE and Mars Odyssey).

This paper is based on observations made with the following facilities: the European Southern Observatory telescopes (Chile) obtained from the ESO/ST-ECF Science Archive Facility (Prog ID. 074.D-0161A), the 10 m Keck I telescope at the W. M. Keck Observatory (Hawaii), the robotic 1.5 M telescope at Palomar Observatory (California), the Italian National Telescope Galileo (La Palma), the 1.82 m Copernico telescope of the Asiago Observatory (Italy), the 2.3 m Advanced Technology Telescope at the Siding Spring Observatory (Australia), the 1 m telescope at the Wise Observatory (Israel), the Subaru 8.2 m telescope of the National Astronomic Observatory of Japan (Hawaii), KAIT and the Shane 3 m telescope at Lick Observatory (California), and the 1.5 m telescope at the Fred Lawrence Whipple Observatory (Arizona). We are grateful to the staffs at all of the telescopes for their assistance. The W. M. Keck Observatory is operated as a scientific partnership among the California Institute of Technology, the University of California, and the National Aeronautics and Space Administration; the Observatory was made possible by the generous financial support of the W. M. Keck Foundation.

REFERENCES

Alard, C. 2000, A&AS, 144, 363

Arnett, W. D. 1982, ApJ, 253, 785

Benetti, S., et al. 2005, ApJ, 623, 1011

Benetti, S., Cappellaro, E., Turatto, M., Taubenberger, S., Harutyunyan, A., & Valenti, S. 2006, ApJ, 653, L129

Bessell, M. S. 1983, PASP, 95, 480

Bloom, J. S., et al. 2002, ApJL, 572, L45

Branch, D., Jeffery, D. J., Young, T. R., & Baron, E. 2006, PASP, 118, 791

Burket, J., Swift, B., & Li, W. 2003, IAU Circular 8232

Buser, R., & Kurucz, R. L. 1978, A&A, 70, 555

Campana, S., et al. 2006, Nature, 442, 1008

Cappellaro, E., Mazzali, P. A., Benetti, S., Danziger, I. J., Turatto, M., Della Valle, M., & Patat, F. 1997, A&A, 328, 203

Clocchiatti, A., Wheeler, J. C., Brotherton, M. S., Cochran, A. L., Wills, D., Barker, E. S., & Turatto, M. 1996, ApJ, 462, 462

Clocchiatti, A., & Wheeler, J. C. 1997, ApJ, 491, 375

Colgate S. A., Fryer, C. L., & Hand, K. P. 1997, in Thermonuclear Supernovae, ed. P. Ruiz-Lapuente, R. Canal, & J. Isern (Dordrecht: Kluwer), p. 273

Elmhamdi, A., Danziger, I. J., Branch, D., Leibundgut, B., Baron, E., & Kirshner, R. P. 2006, A&A , 450, 305

Filippenko, A. V. 1982, PASP, 94, 715

Filippenko, A. V. 1997, ARAA, 35, 309

Filippenko, A. V., Li, W. D., Treffers, R. R., & Modjaz, M. 2001, in Small-Telescope Astronomy on Global Scales, ed. W. P. Chen, C. Lemme, & B. Paczyński (San Francisco: ASP), p. 121

Filippenko, A. V., Foley, R. J., & Swift, B. 2003, IAU Circular 8234

Filippenko, A. V. 2005, in The Fate of the Most Massive Stars, ed. R. Humphreys & K. Stanek (San Francisco: ASP), p. 33

Foley, R. J., et al. 2003, PASP, 115, 1220

Freedman, W. L., et al. 2001, ApJ, 553, 47

Galama, T. J., et al. 1998, Nature, 395, 670

Gal-Yam, A., Ofek, E. O., & Shemmer, O. 2002, MNRAS, 332, L73

Hjorth, J., et al. 2003, Nature, 423, 847

Hurley, K., et al. 2003, GRB Coordinates Network, 2439, 1

Iwamoto, K., et al. 1998, Nature, 395, 672

Iwamoto, K., et al. 2000, ApJ, 534, 660

Kawabata, K., 2007, in preparation

Kennicutt, R. C., Jr. 1998, ARA&A, 36, 189

Krisciunas, K., et al. 2004, AJ, 128, 3034

Landolt, A. U. 1992, AJ, 104, 340

Maeda, K., Nakamura, T., Nomoto, K., Mazzali, P. A., Patat, F., & Hachisu, I. 2002, ApJ, 565, 405

Maeda, K., Mazzali, P. A., Deng, J., Nomoto, K., Yoshii, Y., Tomita, H., & Kobayashi, Y. 2003, ApJ, 593, 931

Maeda, K., Nomoto, K., Mazzali, P. A., & Deng, J. 2006, ApJ, 640, 854

Maeda, K., Mazzali, P. A., & Nomoto, K. 2006, ApJ, 645, 1331

Maeda, K., et al. 2007, ApJ, 658, L5

Maeda, K., et al. submitted

Malesani, D., et al. 2004, ApJL, 609, L5

Mazzali, P. A., Nomoto, K., Patat, F., & Maeda, K. 2001, ApJ, 559, 1047

Mazzali, P. A., et al. 2002, ApJ, 572, L61

Mazzali, P. A., Deng, J., Maeda, K., Nomoto, K., Filippenko, A. V., & Matheson, T. 2004, ApJ, 614, 858

Mazzali, P. A., et al, 2005, Science, 308, 1284

Mazzali, P. A., et al. 2006, Nature, 442, 1018

Mazzali, P. A., et al. 2007, ApJ, 661, 892

Mazzali, P. A., et al. 2007, ArXiv e-prints, 708, arXiv:0708.0966

Mirabal, N., Halpern, J. P., An, D., Thorstensen, J. R., & Terndrup, D. M. 2006, ApJ, 643, L99

Modjaz, M., Kewley, L., Kirshner, R. P., Stanek, K. Z., Challis, P., Garnavich, P. M., Greene, J. E., & Prieto, J. L. 2007, ArXiv Astrophysics e-prints, arXiv:astro-ph/0701246

Nomoto, K., Mazzali, P. A., Nakamura, T., Iwamoto, K., Danziger, I. J., & Patat, F., "Supernovae and Gamma-Ray Bursts: the Greatest Explosions since the Big Bang" ed. Mario Livio, Nino Panagia, Kailash Sahu in Cambridge University Press, ISBN 0-521-79141-3, 2001, p. 144 - 170

Nomoto, K., Tominaga, N., Tanaka, M., Maeda, K., Suzuki, T., Deng, J. S., & Mazzali, P. A. 2007, ArXiv Astrophysics e-prints, arXiv:astro-ph/0702472

Ofek, E. O., Poznanski, D., Gal-Yam, A., & Lipkin, Y. 2003, GRB Coordinates Network, 2434, 1

Pagel, B. E. J., Edmunds, M. G., Blackwell, D. E., Chun, M. S., & Smith, G. 1979, MNRAS, 189, 95

Pandey, S. B., Anupama, G. C., Sagar, R., Bhattacharya, D., Sahu, D. K., & Pandey, J. C. 2003, MNRAS, 340, 375

Pastorello, A., et al. 2006, MNRAS, 370, 1752

Pastorello, A., et al. , in preparation

Patat, F. 1996, PhD thesis, University of Padova

Patat, F., et al. 2001, ApJ, 555, 900

Perlmutter, S., et al. 1997, ApJ, 483, 565

Pettini, M., & Pagel, B. E. J. 2004, MNRAS, 348, L59

Pian, E., et al. 2006, Nature, 442, 1011

Prieto, J. L., Stanek, K. Z., & Beacom, J. F. 2007, ArXiv e-prints, 707, arXiv:0707.0690

Richmond, M. W., et al. 1996, AJ, 111, 327

Richardson, D., Branch, D., & Baron, E. 2006, AJ, 131, 2233

Sauer, D. N., Mazzali, P. A., Deng, J., Valenti, S., Nomoto, K., & Filippenko, A. V. 2006, MNRAS, 369, 1939

Sauer, D. N., et al., in preparation

Schlegel, D. J., Finkbeiner, D. P., & Davis, M. 1998, ApJ, 500, 525

Sharina, M. E., Karachentsev, I. D., & Tikhonov, N. A. 1996, A&AS, 119, 499

Soderberg, A. M., et al. 2006, Nature, 442, 1014

Soderberg, A. M., Nakar, E., Berger, E., & Kulkarni, S. R. 2006, ApJ, 638, 930

Sollerman, J., et al. 2006, A&A, 454, 503

Spergel, D. N., et al. 2003, ApJS, 148, 175

Stanek, K. Z., et al. 2003, ApJ, 591, L17

Sutherland, P. G., & Wheeler, J. C. 1984, ApJ, 280, 282

Tanaka, M., Maeda, K., Mazzali, P. A., & Nomoto, K. 2007, ArXiv e-prints, 708, arXiv:0708.3242

Taubenberger, S., et al. 2006, MNRAS, 874

Thomas, R. C., Branch, D., Baron, E., Nomoto, K., Li, W., & Filippenko, A. V. 2004, ApJ, 601, 1019

Turatto, M., Benetti, S., & Cappellaro, E. 2003, in From Twlight to Highlight: The Physics of Supernovae, ed. W. Hillebrandt & B. Leibundgut (Berlin: Springer), p. 200

Valenti, S. 2008, in preparation

van den Bergh, S., Li, W., & Filippenko, A. V. 2005, PASP, 117, 773

Yoshii, Y., et al. 2003, ApJ, 592, 467

APPENDIX A: FITTING THE BOLOMETRIC LIGHT CURVES OF SNE IA

Following the prescriptions of Arnett (1982) for the photospheric phase and those of Sutherland et al. (1984) and Cappellaro et al. (1997) for the nebular phase, a simple model was adopted for fitting the bolometric light curves of Type I supernovae (SNe lacking the hydrogen-recombination phase):

• *Photospheric phase* ($t \leqslant 30$ d past explosion): We assume homologous expansion for the ejecta, spherical symmetry, no mixing for Ni, constant optical opacity k_{opt}, small initial radius before explosion ($R_0 \rightarrow 0$), and the diffusion approximation for photons (optically thick ejecta). These assumptions are mainly those proposed by Arnett (1982) for SNe Ia, with the main exception that both ^{56}Ni and ^{56}Co are considered as energy sources. With these assumptions, the luminosity evolution in the photospheric phase is described by the following equation, a function of E_k, M_{Ni}, and M_{ej}:

$$L_{ph}(t) = M_{Ni}e^{-x^2} \times$$
$$\left[(\epsilon_{Ni} - \epsilon_{Co}) \int_0^x A(z)dz + \epsilon_{Co} \int_0^x B(z)dz \right], \qquad (A1)$$

with

$$A(z) = 2ze^{-2zy+z^2} \quad \text{and} \quad B(z) = 2ze^{-2zy+2zs+z^2}, \qquad (A2)$$

where $x \equiv t/\tau_m$, $y \equiv \tau_m/(2\tau_{Ni})$, and $s \equiv (\tau_m(\tau_{Co} - \tau_{Ni})/(2\tau_{Co}\tau_{Ni})$. The energies produced in one second by one gram of ^{56}Ni and ^{56}Co are, respectively, $\epsilon_{Ni} = 3.90 \times 10^{10}$ erg s^{-1} g^{-1} and $\epsilon_{Co} = 6.78 \times 10^9$ erg s^{-1} g^{-1} (Sutherland et al. 1984; Cappellaro et al. 1997).

Let τ_{Ni} and τ_{Co} be the decay time of ^{56}Ni and ^{56}Co, respectively, while τ_m is the time scale of the light curve. With the assumption of a homogeneous density, τ_m is

$$\tau_m = \left(\frac{k_{opt}}{\beta c} \right)^{1/2} \left(\frac{10M_{ej}^3}{3E_k} \right)^{1/4}, \qquad (A3)$$

where $\beta \approx 13.8$ is a constant of integration (Arnett 1982) and k_{opt} is the optical opacity.

• *Nebular phase* ($t \geqslant 60$ d past explosion): During the nebular phase, the light curve is determined by the energy deposition of the $^{56}\text{Ni} \rightarrow {}^{56}\text{Co} \rightarrow {}^{56}\text{Fe}$ radioactive decay chain. The light curve is described by the following equation (Cappellaro et al. 1997; Sutherland et al. 1984):

$$L_{neb}(t) = S^{Ni}(\gamma) + S^{Co}(\gamma) + S^{Co}_{e+}(\gamma) + S^{Co}_{e+}(KE), \qquad (\text{A4})$$

where $S^{Ni}(\gamma)$ is the source energy of the nickel decay,

$$S^{Ni}(\gamma) = M_{Ni}\epsilon_{Ni}e^{-t/\tau_{Ni}}, \qquad (\text{A5})$$

while the other terms are the amount of energy deposited by the radioactive decay of ^{56}Co (81% of the energy is released as γ-rays and 19% as positrons). If $\mathcal{E}$ is the rate of energy production by the ^{56}Co decay,

$$\mathcal{E} = M_{Ni}\epsilon_{Co}(e^{-t/\tau_{Co}} - e^{-t/\tau_{Ni}}), \qquad (\text{A6})$$

then the energy $S^{Co}(\gamma)$ generated by the deposition of γ-rays from ^{56}Co decay can be written as

$$S^{Co}(\gamma) = 0.81 \; \mathcal{E} \; (1 - e^{-(F/t)^2}), \qquad (\text{A7})$$

the amount energy deposited by the γ-rays produced in the positron annihilation $S^{Co}_{e+}(\gamma)$ can be written as

$$S^{Co}_{e+}(\gamma) = 0.164 \; \mathcal{E} \; (1 - e^{-(F/t)^2})(1 - e^{-(G/t)^2}), \qquad (\text{A8})$$

and the source energy due to the kinetic energy of the positrons $S^{Co}_{e+}(KE)$ can be written as

$$S^{Co}_{e+}(KE) = 0.036 \; \mathcal{E} \; (1 - e^{-(G/t)^2}) \qquad (\text{A9})$$

The incomplete trapping of γ-rays and positrons is taken into account in the terms $(1 - e^{-(F/t)^2})$ and $(1 - e^{-(G/t)^2})$. Under the assumption of homologous expansion, the absorption probability for γ-ray photons can be approximated by $(1 - e^{-(F/t)^2})$ and the annihilation probability for positrons can be approximated by $(1 - e^{-(G/t)^2})$ (Clocchiatti & Wheeler 1997). The parameters F and G are functions of the ejected mass, kinetic energy, and opacity (Clocchiatti & Wheeler 1997):

$$F = \sqrt{\left(C(\rho)k_\gamma M_{ej}^2\right)/E_k}, \qquad (\text{A10})$$

$$G = \sqrt{\left(C(\rho)k_{e+} M_{ej}^2\right)/E_k} \qquad (\text{A11})$$

where $C(\rho)$ is a function of the density ρ. Using a homogeneous density, $k_\gamma = 0.027$, and $k_{e+} = 7$ (Clocchiatti & Wheeler 1997), $F \approx 32M_{ej}/\sqrt{E_{51}}$ and $G \approx 515M_{ej}/\sqrt{E_{51}} = 16.1F$ (see also Colgate et al 1997).

Using the information coming from the fits to the photospheric and nebular phases, we obtain a rough estimate of the main physical parameters of the SN, without developing a specific model for each object. This simple model gives a good fit to the bolometric light curves of SNe Ia (see Fig. A1), while the two-component model described in §9 is needed for SNe Ic.
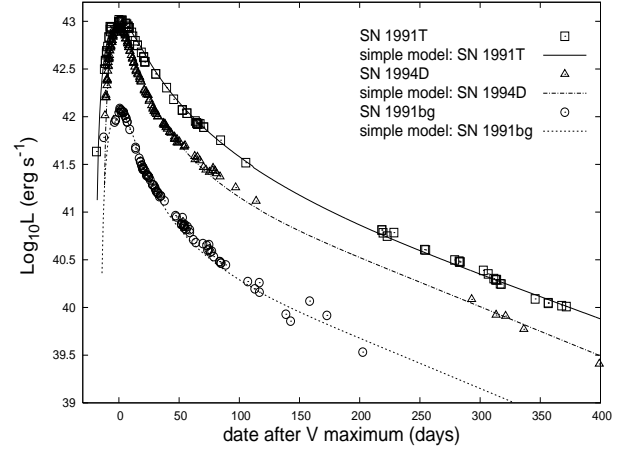

Figure A1. Fit of the quasi-bolometric light curves of three SNe Ia with the simple model.